A NEW MODEL OF THE GLOBAL BIOGEOCHEMICAL CYCLE OF CARBONYL SULFIDE, PART 2: USE OF CARBONYL SULFIDE TO CONSTRAIN GROSS PRIMARY PRODUCTIVITY IN CURRENT VEGETATION MODELS

T. Launois[1,2], P. Peylin[1], S. Belviso[1], B. Poulter[1]

[1] Laboratoire des Sciences du Climat et de l'Environnement (LSCE), IPSL, CEA, CNRS, UVSQ, CE Saclay, Bât 701 L'Orme des Merisiers, 91191, Gif-sur-Yvette, France

Correspondence to: T. Launois (thomas.launois@lsce.ipsl.fr)

[2] Now at INRA, UMR 1391 ISPA, 33140 Villenave d'Ornon, France (thomas.launois@bordeaux.inra.fr)

Abstract

Clear analogies between carbonyl sulfide (OCS) and carbon dioxide (CO_2) diffusion pathways through leaves have been revealed by experimental studies with plant uptake playing an important role for the atmospheric budget of both species. Here we use atmospheric OCS to evaluate the gross primary production (GPP) of three dynamic global vegetation models (LPJ, NCAR-CLM4 and ORCHIDEE). Vegetation uptake of OCS is modeled as a linear function of GPP and leaf relative uptake (LRU), the ratio of OCS to CO_2 deposition velocities of plants. New parameterizations for the non-photosynthetic sinks (oxic soils, atmospheric oxidation) and biogenic sources (oceans and anoxic soils) of OCS are also provided. Despite new large oceanic emissions, global OCS budgets created with each vegetation model show exceeding sinks by several hundreds of GgS yr^{-1}. An inversion of the surface fluxes (optimization of a global scalar which accounts for flux uncertainties) led to balanced OCS global budgets, as atmospheric measurements suggest, mainly by drastic reduction (up to -50%) in soil and vegetation uptakes.

The amplitude of variations in atmospheric OCS mixing ratios is mainly dictated by the vegetation sink over the Northern Hemisphere. This allows for bias recognition in the GPP representations of the three selected models. Main bias patterns are i) the terrestrial GPP of ORCHIDEE at high Northern latitudes is currently over-estimated, ii) the seasonal variations of the GPP are out of phase in the NCAR-CLM4 model, showing a maximum carbon uptake too early in spring in the northernmost ecosystems, iii) the overall amplitude of the seasonal variations of GPP in NCAR-CLM4 is too small, and iv) for the LPJ model, the GPP is slightly out of phase for northernmost ecosystems and

1 the respiration fluxes might be too large in summer in the Northern Hemisphere. These results rely on the robustness of the OCS modeling framework and in particular the

2 choice of the LRU values (assumed constant in time) and the parameterization of soil OCS uptake with small seasonal variations. Refined optimization with regional-scale

3 and seasonally varying coefficients might help to test some of these hypothesis.

1 Introduction

5 The continental biosphere is an integral component of the climate system, and of the carbon and water cycles: it has absorbed about a quarter of the CO_2 released into the

6 atmosphere by anthropogenic activities (Working Group I Contribution to the IPCC Fifth Assessment Report (AR5), Climate Change 2013: The Physical Science Basis) and

7 it modulates the water balance over land. The functioning of the terrestrial biosphere can be heavily affected by climate change in particular by the assumed increase in

8 climate extreme events (Grace and Rayment, 2000; Piovesan and Adams, 2000; Ciais et al., 2005; Schaphoff et al., 2006, Poulter et al., 2014). These events have the potential

9 to reduce photosynthesis or increase ecosystem respiration (e.g., the impact of the European heatwave in 2003 addressed by Ciais et al., 2005). Quantifying carbon storage by

10 ecosystems and predicting their sensitivity to future climate change relies heavily on our ability to diagnose the separate fluxes of photosynthesis and respiration at different

11 scales. Terrestrial gross primary productivity (GPP) remains poorly constrained at global scales, with recent estimates differing by 30-40 Pg C yr^{-1} (Beer et al., 2010; Sitch et

12 al., in prep).

13 The net flux exchanged by an ecosystem (NEE) can be measured continuously by the eddy-correlation technique at site level. However, GPP is not directly measurable.

14 Indirect approaches have been proposed to estimate the biospheric gross fluxes (GPP and respiration): for instance, by using differences between nighttime and daytime NEE

15 measurements (Reichstein et al., 2005, Lasslop et al, 2010) or combining different tracers including stable isotopologues of CO_2 (^{13}C and ^{18}O) (Knohl et al., 2005; Scartazza et

16 al., 2004; Wingate et al., 2010). However, the underlying hypotheses in these approaches impose limitations, especially the poor knowledge of the isotopic signatures of

17 different gross fluxes and their temporal variations when using ^{13}C and ^{18}O data. Moreover, when local measurements are used to calibrate or compare with large-scale

18 estimates, the process of extrapolation creates further uncertainty.

19 Carbonyl sulfide (OCS) is now measured at several atmospheric monitoring stations, and its use as a tracer promises to bring new constraints on the gross fluxes of CO_2. The

20 concept is based on the absorption of OCS by vegetation being directly linked to that of CO_2. Although there is compelling evidence that OCS uptake at the leaf scale is

21 essentially a one-way process (Sandoval-Soto, 2005; Seibt et al., 2010), the link between OCS absorption and photosynthesis is more complex than expected because OCS

22 absorption also takes place during the night and because the leaf relative uptake ratios of OCS and CO_2 during photosynthesis vary with light level (Maseyk et al., 2014). At

23 larger scales (ecosystems, regions or continents), the link between OCS absorption and photosynthesis is also weaker than expected because soils take up atmospheric OCS

too and can turn from a net sink to a net source, depending on whether or not they are saturated. If atmospheric OCS data are to be used to constraint fluxes in global modeling studies, there is no other option than to characterize the spatio-temporal variations in sources and sinks of this gas (Kettle et al., 2002, Suntharalingam et al., 2008, Berry et al., 2013).

Atmospheric records of OCS mixing ratios exhibit clear seasonal variations. Maximal and minimal values for OCS concentrations are observed in winter and late summer, respectively, and the seasonal variations of OCS are highly correlated with those of CO_2 (Montzka et al., 2004).

Here, we use OCS to constrain the annual, seasonal and spatial variations of GPP of three dynamic global vegetation models (DGVMs): LPJ (Sitch et al., 2003), NCAR-CLM4 (hereafter referred to as CLM4CN) (Thornton et al., 2007), and ORCHIDEE (hereafter referred to as ORC) (Krinner et al., 2005). These DGVMs exhibit contrasting global photosynthetic carbon fluxes (120, 130 and 160 Pg C yr^{-1}, respectively). The differences in GPP involve not only the annual global total but also the phase and amplitude of the seasonal variations. All three tested DGVMs were chosen according to the results of the TRENDY experiment, which compared trends in global and regional CO_2 fluxes over the last two decades (TRENDY experiment, Sitch et al., in prep.). For this, we modeled the vegetation OCS sink as proportional to GPP and the leaf relative uptake (LRU), where LRUs were taken from the inventory of Seibt et al. (2010), together with new parameterizations of the non-photosynthetic sinks of OCS (oxic soils and atmospheric oxidation) and of its biogenic emissions (from oceans and anoxic soils). To evaluate our current understanding and representation accuracy of the OCS biogeochemical cycle and quantify the relative impact of each surface flux, we transported those fluxes using the atmospheric LMDz transport model and compared simulated OCS atmospheric concentrations to observations from a database assembled by NOAA/ESRL. In the next step, we define uncertainties associated with each surface flux and optimized these fluxes with an inverse modeling approach to minimize the difference in OCS atmospheric concentrations between simulations and observations.

With the results of these simulations, we successively investigate the following questions:

1. How does our revised parameterization of surface fluxes (oceanic emissions, soil and leaf uptakes) match with the temporal and spatial variations of atmospheric OCS?

2. What is the sensitivity of the phase and amplitude of the simulated seasonal cycles and the sensitivity of the latitudinal gradient of OCS concentrations to changes in surface fluxes?

3. Given the current uncertainties in the surface fluxes, how well would optimized fluxes match with the observed time series of atmospheric OCS?

4. Can we use the OCS atmospheric observations to benchmark the GPP simulated by current DGVMs, given the uncertainties in OCS surface processes?

In the first section, we describe our new set of tropospheric global sources and sinks of OCS and discuss the spatial and temporal distribution of the fluxes. In the second section, we investigate the resulting OCS atmospheric concentration using a forward modeling approach. We then analyze the results of the inverse approach in terms of model-data fit and impact on the fluxes. We finally discuss the potential constraint from these results on the GPP of each DGVM.

2 Material and methods

2.1 Atmospheric OCS and CO_2 observations

Atmospheric OCS and CO_2 concentrations used in this work are from the NOAA/ESRL (National Oceanic and Atmospheric Administration/Earth System Research Laboratory/Global Monitoring Division Flask Program) database, where OCS measurements from 10 stations have been gathered since 2000 (Montzka et al., 2004). These stations include 9 background sites (SPO, South Pole; CGO, Cape Grim, Tasmania, Australia; SMO, American Samoa; MLO, Mauna Loa, Hawaii, United States; NWR, Niwot Ridge, Colorado, United States; BRW, Barrow, Alaska, United States; ALT, Alert, Nunavut, Canada; MHD, Mace Head, Ireland; KUM, Cape Kumukahi, Hawaii, United States) and a single continental site (LEF, Wisconsin, United States). The location of stations is shown in Fig. 1.

Samples were analyzed using gas chromatography and mass spectrometry. OCS data are available for the scientific community at ftp://ftp.cmdl.noaa.gov/data/hats/carbonylsulfide. The typical measurement error for OCS is around 6. ppt, a value much lower than the transport model error. CO_2 data used in this study were downloaded from ftp://ftp.cmdl.noaa.gov/ccg/co2/. For CO_2, we assumed a typical 0.1 ppm measurement error on the observations. More details of the OCS and CO_2 measurement techniques are given by Montzka et al. (2004).

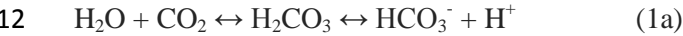### 2.2 The different surface OCS fluxes and their representation in models

Sea-to-air emissions of OCS

1   OCS is emitted from the oceans to the atmosphere either directly, because surface waters are generally supersaturated in OCS, or indirectly through oxidation of atmospheric

2   dimethylsulfide (DMS) and carbon disulfide (CS_2) which are both produced in the surface layer of the ocean. Oceans are a major source of OCS (Kettle et al., 2002). Berry et

3   al. (2013) found that the marine source accounted for 876 Gg S yr^{-1}, about 74% of total sources, but this estimate was not well constrained since the authors increased the

4   direct marine emissions of Kettle et al. (2002) by 600 Gg S yr^{-1} to provide a balanced global budget of OCS (Table 2).

5   Here, the direct emissions are based on parameterizations of ocean production and removal processes of OCS implemented in the NEMO-PISCES oceanic general circulation

6   and biogeochemistry model (Launois et al., 2014). These parameterizations lead to a direct ocean emission of 813 Gg S yr^{-1}. We further accounted for indirect emissions of

7   OCS both from DMS and from CS_2. Details of the parameterizations for the direct and indirect ocean emissions are provided in the appendix, section A.1. Note that for the

8   optimizations, we scaled the standard direct and indirect emissions within a range of variation of -30 – 50 %.

9   **Leaf uptake of OCS**

10   OCS and CO_2 both diffuse through plant stomata into the leaves. CO_2 and OCS are both hydrated in leaves by the carbonic anhydrase enzyme (Protoschill-Krebs and

11   Kesselmeier, 1992; Protoschill-Krebs et al., 1995 and 1996; Stimler et al., 2010), following the reactions:

12     $H_2O + CO_2 \leftrightarrow H_2CO_3 \leftrightarrow HCO_3^- + H^+$ (1a)

13     $OCS + H_2O \leftrightarrow HCOOS^- + H^+ \leftrightarrow H_2S + CO_2$ (1b)

14   Since HCOOS$^-$ and H_2S are found at very low concentrations in plant cells and soil water (Stimler et al., 2010) and that H_2S formation is exergonic, thus spontaneous, the

15   hydration of OCS leads irreversibly to the formation of H_2S (Schenk et al., 2004). Irreversible hydrolysis of OCS is therefore expected within leaves during photosynthesis

16   (Wöhlfahrt et al., 2012; Simmons et al., 1999; Stimler et al., 2010). OCS and CO_2 are both potential substrates for RuBisCO, but CO_2 is favored over OCS by a factor 110 for

17   species studied by Lorimer and Pierce (1989). Stimler et al. (2010) noted that no significant cross-inhibition was measured between OCS and CO_2 uptakes.

18   Different approaches can be used to model leaf uptake of OCS, from process-based formulations with an explicit representation of diffusion and hydration of OCS as in Berry

19   et al. (2013) to more simple parameterizations where the uptake of OCS is expressed as a linear function of GPP:

20     $F_{OCS} = k_{plant\_uptake} * (k_{LRU} * GPP)$ (2),

1   where k_{LRU} is the leaf relative uptake of OCS compared to CO_2 (normalized by their ambient concentrations) and defined for different plant functional type. K_{LRU} is species-

2   specific and several studies have focused on the quantification of this coefficient (Sandoval-Soto et al. 2005, 2012; Stimler et al., 2010; Seibt et al., 2010). We took this later

3   approach with K_{LRU} values from Seibt et al. 2010. We also added a global scaling parameter, k_{plant_uptake}, to further optimize the relative OCS to CO_2 uptake through the

4   inversion scheme. Set to an initial value of one, k_{plant_uptake} is allowed to vary in the optimization from 0.5 to 1.5, representing a +/-50% uncertainty range on initial estimate of

5   surface fluxes (Table 1). Note that the K_{LRU} values from Seibt et al. are in the upper range of recent estimates. Few more details about the implementation of this

6   parameterization can be found in the appendix A.2.

7

8   OCS uptake by oxic soils

9   The general picture is that oxic soils are a sink of OCS while anoxic soils are a source (Whelan et al., 2013).

10   OCS uptake by oxic soils is believed to be essentially a microbial and enzymatically driven process with carbonic anhydrase and OCS hydrolases playing central roles (Chin

11   and Davis, 1993a and 1993b; Seibt et al., 2006; Wingate et al., 2008; Ogawa et al., 2013). There are also clear indications that OCS soil uptake varies according to soil type,

12   temperature and soil water content (Kesselmeier et al., 1999; Van Diest and Kesselmeier, 2008). Previous studies used different approaches based either on temperature and

13   water content (Kettle et al. 2002) or on soil heterotrophic respiration (which tracks microbial activity) and the fraction of water filled pore space (Berry et al. 2013). Here we

14   propose a new approach, based on observed co-variations of OCS and di-hydrogen (H_2) deposition to soils and the existence of global H_2 deposition maps. Consequently,

15   OCS uptake by soil is represented in our model as:

16    $F_{OCS} = k_{soil} * v_{H2} * v_{\_cos\_v_{H2}} * [OCS]_{atm}$ (3)

17   where v_{H2} is the deposition velocity of H_2 into the soil (cm s^{-1}), $v_{\_cos}v_{H2}$ the relative ratio of OCS and H_2 deposition velocities and $[OCS]_{atm}$ the atmospheric concentration of

18   OCS (in ppt). v_{cos}/v_{H2} was set to an initial value of 0.75 in the standard run (following Belviso et al., 2013 and Chen et al., personal communication). As for leaf uptake, a

19   scaling parameter, k_{soil}, is added to optimize the global uptake of OCS by soils. Details about the overall approach and the global H_2 deposition fluxes (taken from a model

20   simulation (Morfopoulos et al. 2012) for our standard simulations and from Bousquet et al. (2011) for tests) can be found in appendix A.3. Given the uncertainties associated

21   with the v_{H2} estimates and the ratio v_{cos}/v_{H2} the surface fluxes were further optimized with a 30% range of variation for k_{soil} coefficient (Table 3).

22

1   **Release of OCS from anoxic soil and wetlands**

2   The role of soils in the OCS budget was recently reviewed by Whelan et al. (2013), with special attention to anoxic soils. The authors underlined the major influence of soil

3   temperature and flooding on OCS emissions from anoxic soils and wetlands. Therefore, we followed their approach but used a model simulation for the spatial and temporal

4   distributions of anoxic soils (from Wania et al., 2010). More details on this OCS source can be found in appendix A.4. For optimization purpose, we defined a scaling

5   parameter, k_{anoxic_soil}, (set to a prior value of one) that is optimized with an assigned +/- 30% variation range (Table 1).

6

7   **Other sources and sinks**

8   Other sources are related to biomass burning and anthropogenic emissions. OCS emissions from biomass burning were simulated from the gridded CO_2 emission maps of Van

9   der Werf et al. (2010) (GFEDv3 product) rescaled to a source of 70 Gg S yr^{-1}, as estimated by Nguyen et al. (1995). The associated uncertainty (maximum range of variation)

10   was set to ±10%. For the anthropogenic emissions (both direct and indirect) we took the fluxes proposed by Kettle et al. (2002). These fluxes were attributed a ±10%

11   maximum variation in the optimization scheme. Additional direct and indirect emissions of OCS by volcanoes were neglected because they are highly uncertain (Belviso et

12   al., 1986).

13   The removal of atmospheric OCS by OH radicals is also a significant sink of OCS. We used monthly maps of OH radicals concentration (integrated vertically up to the

14   tropopause) from Hauglustaine et al. (1998), to distribute both horizontally and temporally a total annual atmospheric sink of 100 Gg S yr^{-1}, as suggested in previous global

15   budgets (Kettle et al., 2002; Berry et al., 2013). This flux was attributed a ±30% maximum variation in the optimization scheme.

16

17   **2.3 Models used in this study**

18   **Terrestrial biosphere models**

19   For the purpose of this study, three independent dynamical global vegetation models (DGVMs) have been used: LPJ, ORCHIDEE (referred as ORC) and CLM4CN. We used

20   the simulated GPP from each model that was performed for the TRENDY inter-comparison experiment (http://dgvm.ceh.ac.uk/) designed to evaluate global carbon budgets

21   and regional trends of the land carbon sinks over the 1990-2009 period. We took the simulated values over the period 2006-2009 where the models were run with the same 11

climate forcing, variable atmospheric CO_2 concentrations and fixed land cover (as a first order analysis). Details about the DGVMs and the simulations can be found in Sitch et al. (2014); few additional information are available in the appendix section A.5.

Atmospheric transport model

The simulated mixing ratios were obtained using the Global atmospheric Circulation Model (GCM) of the Laboratoire de Météorologie Dynamique (LMDz, version 3; Hourdin et al., 2006). The OCS surface fluxes described above are transported in an offline mode using the LMDz transport model, nudged with wind from the European Centre for Medium-Range Weather Forecasts (ECMWF) reanalysis. The transport model uses a $3.75° \times 2.5°$ (longitude× latitude) horizontal resolution and 19 vertical layers between the surface and the top of the troposphere. LMDz has been previously used in many tracer transport studies (Chevallier et al., 2010; Carouge et al., 2010a and 2010b). In this study we used pre-calculated transport fields, corresponding to the sensitivity of the monthly concentration at each site with respect to the daily surface fluxes for all pixels of the transport grid (see Peylin et al., 2005). These pre-calculated sensitivities were derived from the adjoint of the transport model and were multiplied by the surface fluxes to get the atmospheric OCS concentration. They will also be directly used in the inversion (see below) as the optimization algorithm requires the sensitivity of the concentrations to the surface fluxes.

2.4 Optimization framework

Principle and setup:

An optimization algorithm was used to correct the surface OCS fluxes in order to improve the simulation of atmospheric OCS temporal and spatial gradients. The optimization scheme relies on a Bayesian framework that accounts for prior knowledge of the surface fluxes (Tarantola, 1987). Each flux has been assigned a scalar coefficient **x** (see section 2.2) to account for uncertainties in the calculation of the OCS fluxes. These coefficients are the optimized variables (global scaling factors) for all OCS surface flux components described above. Their optimization will provide a better agreement between modeled and observed atmospheric OCS concentrations. The allowed range of variation for each coefficient, **x,** was determined from an analysis of the uncertainties (see **Sect. 2.2**).

The optimization is based on a 5-year-long simulation covering the 2004-2009 period, long enough to characterize broad atmospheric OCS concentration features (trends and mean seasonal cycles). OCS monthly mean concentrations are used as the observational constraint in the optimization.

1

Implementation:

Assuming a Gaussian probability density function (*PDF*) distribution for the measurement errors, the model structure errors (including flux and transport models) and the model parameter errors (flux scalars), the optimal set of parameters under the Bayesian framework corresponds to the minimum of the following cost function $J(x)$ (Tarantola, 1987):

$$J(x) = (Y - M(x))^T R^{-1}(Y - M(x)) + (x - x_p)^T B^{-1}(x - x_p) \quad (4)$$

Where x are the parameters to be optimized (i.e., the OCS surface flux scalars), x_p their a priori values, Y the vector of observations (i.e., the measured OCS mixing ratios at NOAA sites), $M(x)$ the model outputs (i.e., the OCS mixing ratios simulated with the LMDz transport model). **R** and **B** are error variances/covariances matrices associated to the observations and the parameters, respectively.

Details about the optimization scheme (gradient-based algorithm with imposed range of variation) as well as the set up of the inversions (uncertainties on the observations and parameters) are presented in the appendix A.6. We performed standard optimizations with the OCS leaf uptake derived from each DGVMs and a large range of variation for the scaling parameters but also few additional sensitivity optimizations summarized in section 2.5.

2.5 Experiments and data processing

Forward simulations for OCS

A series of simulations was performed, for which the set ups are summarized in Table 1. We carried out three major runs using the three different DGVMs ("STD_ORC", "STD_LPJ", "STD_CLM4CN", refer to Table 1 for details). We made four sensitivity experiments to the representation of soil OCS uptake (with ORC for plant uptake) varying the H_2 flux from Morfopoulos et al. (2012) ("MORF") to Bousquet et al. (2011) ("BOUSQ") and varying the ratio of OCS to H_2 uptake: "TEST_SOIL_MORF_1:1", "TEST_SOIL_MORF_0.5:1", "TEST_SOIL_BOUSQ_1:1", "TEST_SOIL_BOUSQ_0.5:1". We also made two sensitivity experiments varying the magnitude of the oceanic emissions by +/- 30% ("TEST_OCE_+30" and "TEST_OCE_-30"). The other surface fluxes were kept unchanged in all sensitivity tests.

Forward simulations for CO_2

An additional series of simulations was performed to calculate CO_2 concentrations at the same stations. The LMDz transport model was forced with the net ecosystem carbon fluxes from the same three vegetation models (ORC, LPJ, CLM4CN), using also air-sea exchange from the climatology of Takahashi et al. (2008), biomass burning fluxes from GFEDv3.1 (Van der Werf et al., 2010) and fossil fuel emissions from EDGAR-v4.1 (Marland et al., 1999). Simulations with only the gross ecosystem carbon fluxes (GPP and respiration) were also performed separately, to show the individual impact of the two gross fluxes on the CO_2 seasonal cycle at all stations.

Optimization scenarios for OCS

Optimization experiments of the surface fluxes (optimization of a scaling coefficient for each OCS flux component; see section 2.4) were conducted, based on the three different vegetation models. For each model, we tested five scenarios (see Table 1):

-"OPTIM_H-Er": marine, soil and vegetation fluxes are allowed to vary over a large range (up to 50%)

-"OPTIM_L-Er": marine, soil and vegetation fluxes are allowed to vary over a narrow range (±10%) only,

-"OPTIM_Leaf_ONLY": only leaf fluxes are optimized with a large range of variation,

-"OPTIM_Soil_ONLY": only soil fluxes are optimized with a large range of variation,

-"OPTIM_Ocean_ONLY": only ocean fluxes are optimized with a large range of variation.

See Table 1 for details. All other fluxes (OCS oxidation by OH radicals, emissions from anoxic soils and wetlands, direct and indirect anthropogenic emissions, and emissions from biomass burning) were kept unchanged.

Data processing and analysis

1 Observed and simulated monthly OCS and CO_2 concentrations were processed to derive mean seasonal cycles and mean annual trends. To derive mean seasonal cycles and

2 mean annual trends, raw data were fitted with a function including a polynomial term (1st order) and four harmonics. The residuals of the functions were further smoothed in

3 the Fourier space, using a low pass filter (cutoff frequency of 65 days) to define a so-called smoothed curve (function plus filtered residuals). The mean seasonal cycle is

4 defined from the smoothed curve after subtraction of the polynomial term. The mismatches between simulated and observed concentrations is also analyzed in terms of bias,

5 phase and variance, following the mean square error (MSE) decomposition of Kobayashi and Salam (2000):

$$MSE = (\langle X_i \rangle - \langle X_{i'} \rangle)^2 + (\sigma_i - \sigma_{i'})^2 + 2(\sigma_i * \sigma_{i'})(1 - r)^2 \qquad (5)$$

6 The meaning of the squared data bias is obvious. The second term indicates differences in the fast variability: the lack of correlation (r) between X_i and $X_{i'}$ is an estimator for

7 phase errors.

8

9 **3 Results**

10

11 **3.1 Simulated OCS fluxes**

12 Figure 1 presents the monthly mean emissions and uptakes of OCS by the oceans and the terrestrial biosphere (soils and vegetation) for the months of January and July, as

13 calculated from the new parameterizations presented above. Table 2 describes the corresponding annual fluxes, spatially averaged over oceans and continents.

14

15 **Direct oceanic fluxes of OCS**

16 Following the standard run defined by Launois et al. (2014), oceans emit a yearly total of 813 Gg S (Table 2). The spatial distribution indicates a large tropical ocean source

17 (45% of total OCS emissions). Overall, our simulation provides direct oceanic emissions that are about 20 times larger than those from Kettle et al. (2002) and that are

18 roughly comparable to the estimates from Berry et al. (2013) obtained by an optimization procedure (Table 3). Details about the regional and seasonal distribution of these

19 emissions can be found in the appendix section A.7.

1

Indirect oceanic emissions of OCS

On a yearly and global basis, the oceans are also a net source of DMS and CS_2 to the atmosphere. In NEMO-PISCES, each year 133 GgS of OCS are indirectly injected into the atmosphere from DMS, assuming that 0.7% of the total emissions are converted into OCS. This estimate is in good agreement with that of Kettle et al. (2002). Ocean fluxes of CS_2 rely on those of Kettle et al. (2002), since they are not parameterized in NEMO-PISCES. Globally, CS_2 indirectly brings 81 Gg S yr^{-1} of OCS into the atmosphere, as 87% of the CS_2 is assumed to be oxidized into OCS. For more details, see appendix A.7.

Oxic soil uptake of OCS

As described in section 2.2, the standard run for oxic soil uptake of OCS is obtained using the H_2 monthly soil uptake by Morfopoulos et al. (2012) and 0.75 as the ratio between the deposition velocities of OCS and H_2. The resulting OCS fluxes (see Fig. 1 for January and July maps) range between 0 and 15 pmol m^2 s^{-1}; they lead to a global annual uptake of 510 Gg S (Table 2), that is three times larger than the soil uptake modeled by Kettle et al. (2002) and 40% larger than the one reported by Berry et al. (2013). Using different H_2 flux map (from Bousquet et al., 2011) and ratio between the deposition velocities of OCS and H_2 significantly change the global OCS uptake, its regional distribution and its seasonal variations. More details about the regional distribution of the oxic soil uptake can be found in the appendix A.7.

Anoxic soil fluxes of OCS

The emissions from anoxic soils, as described in section 2.2, mainly take place in the northernmost regions (above 60°N), where fluxes up to 12.5 pmol m^2 s^{-1} were simulated (Fig. 1). Total emissions are estimated to be 101 Gg S on an annual basis (Table 2). OCS emissions by peatlands can turn the extra-tropical regions of the Northern Hemisphere into a net source of OCS in late autumn and winter.

Overall, at a global scale, soils constitute a net sink of OCS. In the Northern Hemisphere our estimated sink is lower than that of Kettle et al. (2002) and that of Berry et al. (2013) where the OCS emissions by anoxic soils were not taken into consideration. Details of the regional and spatial variations of the net OCS soil fluxes can be found in the appendix, A.7.

Plant uptake of OCS

Global maps of OCS mean uptake by plants for the months of January and July constructed from the GPP of the ORC model are shown in Fig. 1 (bottom). Using ORC, plants take up 1335 Gg S yr^{-1} (Table 1), which is a considerably larger sink than that modeled by Kettle et al. (2002) or Berry et al. (2013). This yearly global uptake is strongly model-dependent as shown in Table 2 and Fig. A3. Given the linear dependence of OCS uptake to GPP (Eq. 2) the spatial gradients and the phase and amplitude of the seasonal cycle of OCS plant uptake follow those of the GPP. In particular the seasonal cycle shows a distinct peak at high latitudes. Differences between the GPP of the three models are large, especially in terms of amplitude(60% difference between the models) and to a small extend in terms of phase of the seasonal cycle (1 month-shift) (see Fig. A3 for integrated values over latitudinal bands of the Northern Hemisphere). Main spatial and temporal pattern differences are discussed in the appendix A.7.

Other sources and sinks of OCS

An OCS sink of about 100 Gg S yr^{-1} representing photochemical oxidation by OH radicals was implemented, (see section 2.2). The global annual destruction of OCS is relatively evenly distributed, with seasonal variations higher at high latitudes than in the tropics.

The direct and indirect anthropogenic fluxes were taken from Kettle et al. (2002), who estimated that 180 Gg S are emitted on an annual basis, without strong seasonal variations. Eastern Asia, eastern Europe and the eastern parts of Canada and the United States of America concentrate most of the emissions.

As described in section 2.2, the OCS emissions from biomass burning are proportional to the emissions of CO_2, and therefore 60% of the global emissions come from tropical regions..

Global budget of OCS

Table 2 provides an overview of the global sources and sinks of OCS, Only Kettle et al. (2002) and Berry et al. (2013) have provided balanced budgets between sources and sinks, but it is worth remembering that Berry et al. (2013) artificially increased the marine emissions of Kettle et al. (2002) by 600 Gg S yr^{-1} for this purpose. Other global budgets including ours are largely unbalanced, with sinks exceeding sources by hundreds of Gg S yr^{-1}. The budget of Montzka et al. (2007) and the one we derived using ORC's GPPs are the most unbalanced (-776 and -566 Gg S yr^{-1}, respectively).

3.2 Simulated atmospheric OCS concentrations

We transported the simulated OCS surface fluxes with LMDz in a forward approach: the resulting global monthly 3D fields of atmospheric OCS mixing ratios have been compared with in situ observations from the NOAA atmospheric network. Special attention was paid to the annual, seasonal and latitudinal variations of this gas.

Annual trends

Figure 2 compares the simulated monthly mean atmospheric OCS concentrations with the observations at Mauna Loa (MLO), a mid-latitudinal background station in the middle of the tropical Pacific Ocean (20°N, altitude 3500 m). This site therefore represents the integrated contribution of the surface fluxes from the entire Northern Hemisphere (Conway et al., 1994). Since the three global budgets (with the three DGVMs) are not balanced with large sinks (Table 2), the simulations show large negative annual trends of the atmospheric OCS concentrations (23 to 70 ppt yr^{-1}), which are inconsistent with the observations. Kettle et al. (2002) proposed a roughly balanced OCS budget but with too small seasonal variations when compared with the observations. The situation at South Pole (SPO) resembles that at MLO in terms of annual trends (Fig. 3)

Results of sensitivity tests on the ocean OCS source (see section 2.5) are displayed in figure 3. Changing by +/- 30% the ocean source significantly impacts the simulated trend and only marginally the phase and amplitude of the seasonal cycle (except at SPO). In the case of ORC, the test "TEST_OCE_+30" provides a global budget close to equilibrium..

Figure 4 (left panel) shows the impact on the annual trend at MLO of four sensitivity tests on the calculation of oxic soils OCS uptake (see section 2.5). The annual trend is more affected by changes in v_{OCS}/v_{H2} ratios (25 ppt yr^{-1} between the the 1:1 and 0.5:1 ratios) than by changes in the way H_2 deposition velocities have been estimated (10 ppt yr^{-1} difference between the "TEST_SOIL_MORF" and "TEST_SOIL_BOUQ" simulations). However, changes in OCS uptake by oxic soils cannot compensate entirely for the strong negative trend imposed by the vegetation sink deduced from ORC GPP.

Simulated phase and amplitude of the seasonal variations

Figure 5 (right panels) compares the smooth seasonal cycle of OCS concentrations of three different simulations, the concentrations deduced from Kettle inventory and and the observations at the South Pole (SPO), Alert (ALT) and MLO stations. The ALT data help in exploring the influence of boreal and temperate ecosystems of the Northern

1 Hemisphere on the biogeochemical cycle of OCS, while SPO station combines the southern ocean and land influences. The simulation based on Kettle et al. (2002) fluxes

2 exhibits amplitudes which are unrealistically low and not in phase with the observations at ALT and MLO. At SPO, on the contrary, Kettle et al. (2002) fluxes produce a good

3 fit to the observations, both in terms of seasonal amplitude and phase. At SPO, our three models simulate slightly larger amplitudes (+ 10-15 ppt relative to observations) and

4 a slight shift in the OCS maximum during austral summer.

5 The ORC model displays the highest seasonal amplitudes both at ALT and MLO where the northern vegetation influence is dominating the seasonal variations (around 250

6 and 80 ppt, respectively). These variations are unrealistically high compared to the observations (100 ppt and 55 ppt, respectively). However, ORC shows seasonal OCS

7 variations more in phase with the observations than when using the two other DGVM's GPP, especially at ALT. Using CLM4CN leads to the right amplitude of the seasonal

8 variations in OCS concentrations at ALT, but the phase is incorrectly represented (earlier OCS build-up and draw-down). This model provides a better representation of the

9 phase of the OCS cycle at MLO but leads to a 10% underestimation of the OCS seasonal amplitude at this station. Data shown in the right panels of Fig. 3 and Fig. 4 aim at

10 characterizing the sensitivity of seasonal variations to changes solely in marine emissions and in the soil sink, respectively (following sensitivity experiments described in

11 2.5). At MLO, both the phase and the amplitude of the seasonal variations are unaffected by changes in marine emissions (Fig. 3) or oxic soils uptake (Fig. 4). At SPO, a 30%

12 increase of the ocean flux leads to about 10% increase in amplitude of the seasonal variations (Fig. 3). Similar experiments were conducted to evaluate the contribution of

13 plant uptake on the overall seasonality of atmospheric OCS (runs where only the plant uptake is transported). Figure 6 shows that the amplitude and the phase of the seasonal

14 variations at ALT and MLO are both primarily determined by the uptake of OCS by vegetation. On the other hand, plant uptake plays a little role on the seasonality at SPO.

15

16 **Annual mean atmospheric concentrations of OCS: north-south gradients**

17 Annual mean mixing ratios for the 10 stations of the NOAA monitoring network, plotted as a function of latitude, are shown in Fig. 7. Note that the simulated global mean

18 OCS concentration (across all sites) has been rescaled to the observed global mean, so that only the gradients between stations should be investigated. The main results from

19 this diagnosis are:

20 1.   Our new OCS surface flux scenarios capture the main differences in annual mean concentration between stations with lower concentrations at continental stations in

21   the Northern Hemisphere (LEF, BRW, ALT) than at background stations as in the Southern Hemisphere (around 50 ppt lower),

2. Observed differences between southern extra-tropical marine stations and tropical marine stations (higher concentration over the tropics by 10 ppt) are also represented by the different scenarios,

3. Significant discrepancies still affect all scenarios, such as for instance, the difference between NWR and LEF, with simulated values around 25 to 30 ppt compared to observed ones around 60 ppt,

4. There are small but significant differences between the three scenarios based on three different ecosystem models. For instance, between Cape Grim (CGO) and American Samoa (SMO), although all models largely overestimate the mean concentration gradient, using CLM4CN reduces it by nearly 20 ppt compared to ORC. Similarly, CLM4CN gives a lower annual mean concentration at Point Barrow (BRW) than at Alert (ALT) while the two others models give higher concentrations at BRW, in line with the observations,

5. The simulation based on the Kettle et al. fluxes (2002) shows much smaller annual mean gradients across stations than our three scenarios. The better match between the observed gradients and our new flux scenarios partly arises thanks to the re-estimated high oceanic emissions in the tropical regions.

The two sensitivity tests, where ocean emission and soil uptake were increased by 30% (TEST_OCEAN_+30 and TEST_SOIL_MORF_1:1, respectively) have little influence on the atmospheric mixing ratios when compared with the "STD_ORC" run (Fig. 7, dotted and dashed lines).

3.3 Results of the optimization: OCS concentrations and surface fluxes

Each surface flux component has been scaled with an optimization procedure (see section 2.4 and 2.5) in order to obtain the best fit to the atmospheric OCS concentrations (raw data). We investigate whether the observed temporal and spatial OCS variations can be matched through the optimization and highlight corrections on the GPP and other fluxes that would be needed. Table 3 summarizes the initial and the optimized values of the surface fluxes for the different optimization configurations.

Optimization of the annual trends

1   The OCS monthly mean concentrations simulated with the optimized surface fluxes of the "OPTIM_H-Er" scenario (large range of variation for the optimized parameters) are

2   shown in Fig. 8. Allowing a 50% range of variation on the surface fluxes is sufficient to yield equilibrated global budgets after optimization, in agreement with the

3   observations (see the last line of Table 3). Overall, the total sink is decreased in all optimization results, from an average value (all three DGVMs included) of 1721 Gg S yr^{-1}

4   in the prior simulation to 1218 Gg S yr^{-1} after optimization, thus a 29% reduction. The source flux estimates were also reduced by 13% on average, from 1379 Gg S yr^{-1} in the

5   prior simulation to 1204 Gg S yr^{-1} after the optimization. The new simulated global budgets are almost balanced (-1 to -20 Gg S yr^{-1}) and the annual trend significantly

6   reduced (Fig. 8 versus Fig. 2), especially for ORC (-566 to -10 Gg S yr^{-1}).

7   The soil uptake of OCS is reduced as much as 45%, even if the maximum range of variation allowed is 50%. The leaf uptake of OCS is also not reduced up to the limit when

8   allowing a range of variation of 50%. On average, vegetation and soil optimized uptakes are respectively converging around 714 and 396 Gg S yr^{-1} (Table 3). The atmospheric

9   destruction of OCS by OH radicals and some sources were also optimized at their maximum allowed values (e.g emissions by anoxic soils, indirect oceanic emissions and

10 indirect anthropogenic emissions).

11 In the low variation range scenario ("OPTIM_L-Er"), a negative trend of about 30 ppt yr^{-1} remains with ORC (Fig. 8). This "OPTIM_L-Er" configuration could be thought as

12 a theoretical case where the values of k$_{LRU}$ (for OCS leaf uptake) would be well constrained as well as the fluxes controlled by soil, ocean and anthropogenic processes. In this

13 theoretical case, the mismatch between the simulated and observed annual trend for ORC would suggest that:

14 1.   the vegetation plays a determinant role in the OCS global atmospheric budget

15 2.   the leaf uptake of OCS is too large when using ORC, highlighting a too large global annual GPP flux.

16 In reality, the LRU values (taken from Seibt et al., 2006) are likely to be too large so that the conclusion on the GPP of ORC cannot be inferred yet with the OCS budget only.

17

18 **Optimization of the amplitude and phase of the seasonal variations**

19 Figure 9 shows the OCS mean seasonal cycles before and after optimization using the three DGVMs. At most NOAA stations, the optimization of the surface fluxes

20 significantly improves the simulated seasonal amplitude of the atmospheric OCS concentrations, with a global reduction of the MSE (in ppt^{2}) from 162 (resp. 83) to 29 (resp.

29) ppt for ORC (resp. LPJ) and from 43 to 35 ppt for CLM4CN. Although all optimizations lead to a significant improvement of the amplitude of the OCS cycle, differences between the three models remain:

1. With the ORC model, the standard "OPTIM_H-Er" configuration strongly reduces the amplitude of the simulated OCS seasonal cycle, especially at high latitudes (e.g., from 225 ppt to 140 ppt at ALT). The resulting amplitudes are more consistent with the observations but are still too large at high latitudes (140 versus 100 ppt at ALT). At MLO, the amplitude of the OCS levels is reduced from 80 to 45 ppt, a value slightly lower than the observations (50 ppt). Finally, we also note that scaling the surface fluxes through the optimization leads to negligible modifications of the phase of the simulated OCS concentrations.

2. With LPJ, the optimization also leads to a reduction of the sources and sinks (Table 3), which decreases the amplitude of the OCS seasonal cycle. Among the three DGVMs, LPJ displays the best fit of the amplitude of the OCS annual cycle at temperate latitudes with the observations. However, the optimization does not improve the phase of the atmospheric OCS signal with, therefore, the same 2-month-early shift of the model at northern stations (ALT and BRW) as for the prior.

3. With CLM4CN, the optimization does not significantly improve the mean seasonal cycle, with too small prior and posterior amplitudes at high northern sites compared to the observations (60% and 75% of the observed cycle amplitude at ALT and MLO, respectively). The phase is also not changed and most discrepancies noticed in section **3.2.2** remain (e.g, two months phase advance at BRW).

Overall the three final sets of optimized fluxes (Table 3) confirm that:

1. The total sink is always reduced, mainly through a decrease of soil uptake and plant uptake.

2. The large direct emissions of OCS by the tropical oceans are decreased by only 15%, with global annual mean around 691 Gg S yr^{-1} (after optimization)

3. New vegetation and soil uptakes respectively around 714 and 396 Gg S yr^{-1} (Table 3) would be needed for fitting the main temporal and spatial variations of atmospheric OCS. These new estimates are in the upper range of previously published global budgets (Table 2).

Optimization of the annual mean north south gradients

18

Figure 10 presents the prior and optimized annual mean OCS mixing ratios at all stations as a function of the latitude. The overall improvements from the optimization are summarized with the mean of the MSE for all sites (see the legend). Posterior MSEs are similar between the three scenarios (around 24 ppt^2) and the reduction between the prior and the posterior MSEs are equivalent to 74%, 31% and 27% for ORC, CLM4CN and LPJ respectively. Note that such improvement is much smaller than for the seasonal cycle where MSE decreases by 82%, 19% and 65%, respectively (see Fig. 9). The large reduction of the soil and leaf OCS uptakes through the optimization (see Table 3) helps reducing initial differences in the spatial gradients between stations. For example, the simulated difference between SPO and CGO stations in the Southern Hemisphere drops from 10-25 ppt to 2-10 ppt in closer agreement with the observations (around 1 ppt).

4 Discussion

Although our revised OCS budgets agree relatively well with the observed temporal and spatial gradients recorded at NOAA stations (using the LMDz transport model), other biases still exist. These biases will be first discussed to highlight potential errors in the OCS leaf, soil and ocean surface fluxes. In a second step, we will review and discuss the constraint brought by OCS on the GPP of the three tested DGVMs, when the information from both OCS and CO_2 tracers are combined.

4.1 Remaining biases in simulated atmospheric OCS concentrations

The standard optimizations ("OPTIM_H-Er") using the three DGVMs provide an equilibrated atmospheric budget, with fluxes for the three most important OCS surface processes converging to similar values (Table 3) across all simulations :leaf and soil mean annual uptake are 714 and 396 Gg S yr^{-1} respectively, ocean source is 691 Gg S yr^{-1}. These values are much larger than those proposed initially by Kettle et al. (2002) and relatively close to the recent budget of Berry et al. (2013). Large gross surface fluxes are needed to simulate the observed seasonal peak-to-peak amplitude at mid/high latitudes of the Northern Hemisphere (around 120 ppt), as highlighted by the optimizations. Note that the study of Berry et al. (2013) further emphasizes the need for large land surface uptake (leaf and soil) if we are to simulate the observed vertical profiles over vegetated areas (especially the observed drawdown of OCS concentrations in boundary layers; see their Fig. 9). On average our ensemble of tests highlights for all three scenarios that: i) uptake through leaves (following GPP) controls the atmospheric seasonal cycle, and ii) uptake by oxic soils, although the second largest sink, has a limited impact on the atmospheric OCS seasonal cycle.

1 We summarize below the performances of different optimization scenarios (based on the three DGVMs) and highlight the remaining discrepancies in terms of simulated

2 trend, amplitude and phase of the seasonal cycle. Figure 11 displays the observed minus modeled trend at MLO (first row), the mean square error (MSE) decomposition

3 (phase, bias and variance; see **§2.5**, Eq. (3)) obtained from the detrended concentrations at ALT and MLO (second and third row) and the amplitude of the seasonal cycle at

4 ALT and MLO (last two rows). The results from several optimization scenarios (based on the three DGVMs) are displayed including prior fluxes ("Pri"), optimized fluxes

5 with high and low uncertainties ("OPTIM_H-Er" and "OPTIM_L-Er"), and three tests where only the leaf, soil or ocean component are optimized (the other components

6 being fixed).

7

8 **Atmospheric trend**

9 As shown in Fig. 11, the optimization successfully corrects the annual trends, for most scenarios. For ORC, the global budget can be closed only if the leaf uptake is decreased

10 by 45%, which is not possible in the low error test. This suggests that LRUs provided by Seibt et al. (2010) are likely too large. Future studies would benefit from using lower

11 LRUs, such as those published in other studies (Sandoval-Soto et al., 2005; Stimler et al., 2012, Berkelhammer et al., 2013). Lower LRU values also correspond to a test in

12 Seibt et al. (2010) where the internal mesophyll conductance is set as the major limitation in the diffusional pathway of OCS (average LRU would be 2.08 with this

13 assumption, instead of 2.8 as used in the present paper). Moreover, several studies have shown that OCS-to-CO_2 uptake ratio could be plant-specific (Sandoval-Soto et al.,

14 2005, Campbell et al., 2008; Seibt et al., 2010; Stimler et al., 2012; Berkelhammer et al., 2013) and even, under certain conditions, that some plants can release some of the

15 absorbed OCS (Xu et al., 2002; Geng et al., 2006; White et al., 2010). Therefore, recent estimates of the vegetation OCS uptake are still largely uncertain and differ by up to a

16 factor of six (Xu et al., 2002; Kettle et al., 2002; Sandoval-Soto et al., 2005; Berry et al., 2013).

17 1.   Optimizing only one flux component is usually enough to correct the trend, except for ORC, pointing out again the likely too high leaf uptake, which can be due to

18   overestimated LRU or too large GPP.

19

20 **Phase and amplitude of the atmospheric seasonal cycles**

21 Looking at the phase component of the MSE decomposition , few general features can be drawn:

1. *1.* On average, only small changes are observed at most sites between prior and posterior estimates (only shown for MLO and ALT, Fig. 11, second and third rows). A 35% reduction of the phase error is noticed at MLO for ORC and also a 25% improvement for LPJ.

2. *2.* These small phase changes result from the optimization of only one global annual scalar for each flux component.

3. *3.* On average, ORC provides, after optimization, the best phase agreement with the observations at high northern latitude stations (see ALT). At MLO the optimized results are closer between the three models, although LPJ and CLM4CN provide slightly better matches with the observations (72 and 70 ppt/year² error respectively, versus 120 ppt^2 for ORC).

4. *4.* Most changes are due to the optimization of the leaf uptake, while "OPTIM_SOIL_ONLY" and "OPTIM_OCEAN_ONLY" configurations do not allow for significant phase improvement.

5. Further improvement of the phase should account for potential variations of LRU through the season, or possible important soil deposition velocity changes through the season, as mentioned in the recent paper by Maseyk et al. (2014). This could be achieved with an optimization of the monthly flux of each component.

The diagnosis of the amplitude of the simulated seasonal cycle corresponds to the last two rows of Fig. 11 and also partly to the variance term of the MSE decomposition. Main features are:

1. The improvement compared with the prior main results from the optimization of the OCS leaf uptake.

2. Smaller or negligible changes are noticed at ALT and MLO stations when only the ocean fluxes are optimized ("OPTIM_OCEAN_ONLY" configuration), but significant improvements can be seen at southernmost stations (10% variance error correction, not shown).

3. When only the soil uptake is optimized ("OPTIM_SOIL_ONLY" configuration), no improvement on the simulated amplitude is obtained.

4. The amplitude is too large in the prior for ORC at both ALT and MLO and remains too large at ALT after optimization, suggesting again that either LRU values or GPP fluxes are too large for high latitude ecosystems. LPJ provides the best compromise in terms of amplitude when we consider all stations. However, the optimization of only one global coefficient for each flux does not allow for corrections of local flux biases, which leads to over- and under-estimated amplitudes at different sites for both LPJ and ORC.

5.   For CLM4CN, the simulated amplitude is too small at most stations, and cannot be corrected through the optimization of a global scaling factor because of the initial phase mismatch.

6.   Finally, one should note that the amplitude of the atmospheric signal also depends on the transport model and potential vertical mixing errors. The version of the LMDz model used here is believed to have too large mixing in the planetary boundary layer (PBL) (Patra et al., 2011, Locatelli et al., 2013), which would thus dampened the amplitude of the seasonal cycle.

Annual mean atmospheric spatial gradients:

We use the bias diagnosis from the MSE decomposition, which also accounts for any remaining trend mismatch, to analyze the annual mean gradients. As demonstrated by the results of the optimization of only one component ("OPTIM_XXX_ONLY" tests), all processes make a similar impact on the annual mean OCS concentrations. However, the optimization scheme leads to a degradation of the bias at MLO for the three models and the bias remains highly variable at other sites. The constraint imposed by the annual mean gradients cannot be significantly improved.through the optimization. The overall fit at some stations can be decreased (see for instance CLM4CN at MLO, Fig. 11) because of compensation by improvements at other sites. When testing the impact of the observation errors on the optimization, including a test with equal observation errors (18 ppt) the results were not substantially modified.

4.2 Joint constraint of atmospheric OCS and CO_2 data to evaluate model GPP

We now analyze and discuss potential constraints on the GPP of each ecosystem model that could be derived from the results of the OCS simulations (direct and inverse) and of additional CO_2 simulations (see methods **§ 2.5**). Figure 5 and 6 display in the right-hand columns the atmospheric CO_2 concentrations simulated with the net CO_2 ecosystem exchange (NEE = GPP - Respiration) from the three DGVMs used for the OCS scenarios (including also standard fossil fuel emissions and ocean fluxes). Figure 5 compares the smoothed temporal variations of the simulated CO_2 and OCS concentrations at three stations (ALT, MLO and SPO). For CO_2, all three models capture the observed seasonal cycle with nevertheless significant biases in terms of amplitude and/or phase, depending on the DGVM. As first described by Montzka et al. (2007), the OCS seasonal patterns are similar to CO_2, but with noticeable differences in the timing of the maximum and minimum. The largest difference is observed at the SPO station with a phase shift of nearly five months between the two tracers. Additionally, Fig. 6 quantifies the contribution of the leaf uptake and of the GPP to the total simulated

22

concentrations, for OCS and CO_2, respectively. In the Northern Hemisphere, the phase and amplitude of the OCS seasonal cycle is primarily driven by the OCS leaf uptake, while for CO_2 the seasonal cycle combines both GPP and respiration fluxes. Our OCS modeling framework thus provides support for a new constraint on GPP. Note, however, that for OCS, the other flux components (mainly the soil uptake and the ocean release) also contribute to the seasonal cycle but with nearly canceling effects.

We now discuss the implications of the simulated OCS and CO_2 biases for each DGVM, separately. We refer to Fig. 12 that displays the normalized amplitude of the simulated OCS seasonal cycle as a function of the normalized amplitude of the simulated CO_2 seasonal cycle at all stations (the normalization is done with respect to the observations).

ORC model:

The analysis of the concentrations at boreal stations provides a first hint on northern high latitude ecosystems. Both OCS and CO_2 simulated seasonal amplitude are too large at ALT (by factors 2 and 1.5, respectively). While the sole CO_2 diagnosis would suggest either too large GPP during boreal summer or a too small amplitude of the respiration seasonal cycle, the additional OCS diagnosis indicates that the GPP of ORC is indeed too large for high latitude ecosystems. For OCS, uncertainties in LRU values also contribute to the model data mismatch. As suggested by Berkelhammer et al. (2013) the LRUs from Seibt et al. (2010) are on the upper range of the different estimates published so far (+ 30% compared to the mean estimates). However, a 45% reduction of the LRU that corresponds to the optimized fluxes of the "INV_H-Er" case (see Table 3) still produces an amplitude of the seasonal cycle at ALT larger than the observation by a factor 1.3 (Fig. 12). Such remaining discrepancy thus confirms that ORC GPP is most likely overestimated at high latitudes. Note that for both tracers the phase of the seasonal cycle is relatively well captured (Fig. 5).

The signal at MLO integrates the contribution from the land (and ocean) fluxes of the whole Northern Hemisphere. In this case, there is a relatively good agreement for the phase and amplitude of the CO_2 seasonal cycle, while for OCS the amplitude is still too large (by a factor of 1.5). This suggests that the chosen LRU values are indeed too large and that the too large GPP for boreal ecosystems, noticed above, may be compensated by too small GPP at mid and low latitudes. The result of the standard optimization leads to the right amplitude at MLO, which further indicates that the 50% global reduction of OCS leaf uptake is sufficient on average to compensate for too high GPP at northern ecosystems and potentially too large LRU.

The seasonal cycle at the remote SPO station is more difficult to interpret as i) the amplitude of the cycle is 8 times smaller than at MLO for CO_2 and ii) all surfaces fluxes (i.e. from leaf, soil, and ocean) have a shared contribution to the overall seasonal cycle. The too large amplitude of ORC for CO_2 reflects discrepancies in both GPP and respiration fluxes, but also in air-sea exchanges.

23

Overall, the joint OCS/CO_2 analysis points towards discrepancies in the ORC GPP, with overestimated values at high northern latitudes. Such conclusion directly corroborates the results obtained by Kuppel et al. (2014), using the same ecosystem model, when optimizing its parameters with eddy-covariance flux measurements (CO_2 and latent heat flux). They proposed a large reduction of the GPP for boreal broadleaf and boreal needleleaf forests.

CLM4CN model:

The amplitude of the seasonal cycle simulated with CLM4CN is underestimated at nearly all stations for both OCS and CO_2, with a modeled-to-observed ratio between 0.6 and 0.9, except at CGO where the amplitude is overestimated (Fig. 12). Moreover, as shown in Fig. 5, the phase shift in the OCS seasonal cycle at boreal stations (i.e., ALT) also occurs for CO_2, with an earlier drawdown of the modeled concentrations compared to the observation (around two months). Such phase shift is much smaller or close to zero at temperate and low latitude stations of the Northern Hemisphere.

The combined OCS and CO_2 discrepancies point toward biases in the CLM4CN simulated gross carbon fluxes. First, the GPP of high northern latitude ecosystems is most likely out of phase, with a too strong increase of photosynthesis in spring. Using only the CO_2 tracer would suggest that one or both gross carbon fluxes are out of phase (photosynthesis and respiration). The benefit of the OCS tracer is to clearly point toward GPP as the major source of discrepancies, given that for OCS the leaf uptake, which is proportional to GPP, drives the overall seasonal cycle (see Fig. 6). Second, the amplitude of the GPP is also most likely underestimated for most ecosystems. While the CO_2 concentrations do not allow to blame the GPP more than the respiration, the OCS points again towards too small a GPP during the peak of the growing season.

Increasing by 20% and shifting by two month the seasonal course of the CLM4CN GPP for high latitudes would create a significant improvement of both OCS and CO_2 simulated concentrations. At SPO, the CO_2 seasonal cycle is in good agreement with the observations, while the OCS seasonal cycle shows too large amplitude and an earlier maximum – similarly with the two other DGVMs.

LPJ model:

Using the GPP from LPJ leads to intermediary results for the seasonal amplitude, for both tracers, with no systematic biases across stations (Fig. 12). If we consider boreal stations, the modeled seasonal amplitude for CO_2 is 20% lower than the observations, while for OCS it is 50% higher. As noticed above, the temporal variation of the OCS concentrations at these sites is slightly out of phase with a too early drawdown in spring. This would suggest that the increase of boreal ecosystems GPP in spring is too early

1   and too strong in LPJ (see for instance Fig. A4 in the appendix). However, matching both OCS and CO_2 atmospheric signals would also require a change in the temporal

2   variation of the ecosystem respiration (to fit the CO_2 signal).

3   At MLO, the phase shift becomes much lower for OCS. The too low amplitude for CO_2 would suggest that either the GPP is underestimated during the peak of the growing

4   season (it is much smaller than when using ORC, see Fig. A4) or that the respiration is too large during summer time. The OCS diagnostic with slightly too large amplitude at

5   MLO (Fig. 5) suggests that: i) the main bias comes from the respiration, and ii) the LRU values from Seibt et al. (2010) are likely overestimated (as already pointed out),

6   which would explain the too large amplitude for OCS. As can be seen in Fig. A4, the LPJ model is the only one with respiration fluxes of the same magnitude as GPP fluxes,

7   in temperate northern regions during mid and late summer. Reducing the intensity of the respiration during this period would allow for larger annual variations of the CO_2

8   concentrations, more consistent with the observations while still keeping the correct GPP-based representation of the OCS leaf uptake.

9

10   Overall, the above joint OCS and CO_2 analysis points towards deficiencies for each model's gross carbon fluxes. The results obtained for the combined OCS-based and CO_2-

11   based analyses are coherent between the three models. For instance, the decrease of ORC GPP for temperate and high latitude ecosystems or the phase-shift of CLM4CN GPP

12   would bring the different GPP estimates close together.. However, some caution is still needed before drawing firm conclusions. For instance we should further investigate:

13   1.   The spatial and temporal variations of the OCS-to-CO_2 uptake ratio (LRU). More recent estimates based on additional in situ measurements are likely to provide

14   lower LRU values than those of Seibt et al. (2010). LRU values have also been proved to vary depending on available light, and therefore to change according to

15   seasons (Maseyk et al., 2014).

16   2.   The seasonality of soil OCS uptake. Our modeling strategy, based on similarities between H_2 and OCS uptake by soils, leads to a relatively small seasonal cycle of the

17   OCS soil flux. Any large modifications of the seasonality of that component would directly impact our conclusions and to a certain extent our diagnostic on the gross

18   carbon fluxes of the three DGVMs.

19   3.   The impact of potential atmospheric transport errors. Indeed the mixing within atmospheric transport model is still subject to significant uncertainties, which in turn

20   may impact the conclusions that are directly linked to the amplitude of the seasonal cycle. Nonetheless, the LMDz model has been used in many tracer transport

21   studies with no strong known biases (Peylin et al., 2014).

22

5 Conclusion

Several studies have proposed a relationship between GPP and a concomitant OCS uptake by the vegetation, which would partly explain the atmospheric OCS concentration variations, yet the observed atmospheric measurements of OCS concentrations have never been used in a quantitative way to obtain information about the GPP of current global vegetation models. In this context, this study proposed a new set of global sources and sinks of OCS, using the GPP from three different global vegetation models to compute the leaf uptake of OCS. We further used the LMDz atmospheric transport model to compute the temporal and spatial gradients of OCS concentration (as well as of CO_2) in the atmosphere.

We proposed a global OCS budget fully based on parameterized processes that include large emissions by the ocean and important uptake by soil and vegetation, After the optimization of all flux components (within given ranges), we obtained a new flux scenario that i) matches the observed OCS trend in the atmosphere (close to zero) and ii) provides a good agreement to the atmospheric concentrations (in terms of amplitude and phase of the seasonal cycle and annual mean gradients). Our modeling framework suggests that the GPP-related uptake of OCS mainly controls the seasonal cycle of atmospheric OCS concentrations, with much smaller influence from ocean and soil fluxes.

More importantly, combining the information from OCS and CO_2 atmospheric observations allowed us to highlight potential biases in the GPP of three dynamic global vegetation models. We showed that: i) for the ORC model, the terrestrial gross carbon fluxes in the Northern Hemisphere high latitudes are currently too large, ii) for the CLM4CN model, the GPP is out of phase with an uptake of carbon by northern high latitude ecosystems that occurs too early in spring, and iii) for the LPJ model, the respiration fluxes might be too large during the peak of the growing season on average in the Northern Hemisphere.

For the first time, our study quantifies the potential of OCS measurements to benchmark gross carbon fluxes from current DGVMs. It also highlights the need to better characterize the different processes that control the surface OCS fluxes and in particular the seasonality of soil uptake. From such preliminary study, we foresee additional and complementary experiments that would:

1. Improve the inversion framework in order to optimize the temporal pattern of each flux component, using for instance a monthly time step optimization. This would provide further information on the potential biases associated to the seasonal variations of the GPP of each model.

2. Combine the different models for the GPP-related uptake of OCS within a single inversion framework, where we would optimize a unique set of LRU coefficients (for each PFT) together with the GPP fluxes of all DGVMs simultaneously.

3. Optimize multi-data streams, based on both atmospheric OCS and CO_2 data. This would allow separate optimization of GPP and respiration, using prior estimates from a given ecosystem model. Optimizing for both tracers would allow us to account for uncertainties associated with the different components of the CO_2 and OCS budgets in the atmosphere simultaneously, relying on the GPP as a shared component.

Acknowledgements

References

Barnes, I., Becker, K. H., Patroescu, I. The tropospheric oxidation of dimethyl sulfide: A new source of carbonyl sulfide. GEOPHYS RES LETT., 21(22), 2389-2392, 1997

Beer, C., Reichstein, M., Tomelleri, E., Ciais, P., Jung, M., Carvalhais, N., Papale, D. (2010). Terrestrial gross carbon dioxide uptake: global distribution and covariation with climate. SCIENCE, 329(5993), 834-838.

Belviso, S., Nguyen, B. C., Allard, P. (1986). Estimate of carbonyl sulfide (OCS) volcanic source strength deduced from OCS/CO2 ratios in volcanic gases. GEOPHYS RES LETT , 13(2), 133-136.

Belviso, S., Masotti, I., Tagliabue, A., Bopp, L., Brockmann, P., Fichot, C., Fukuchi, M. (2012). DMS dynamics in the most oligotrophic subtropical zones of the global ocean. BIOGEOCHEMISTRY, 110(1-3), 215-241.

Belviso, S., Schmidt, M., Yver, C., Ramonet, M., Gros, V., Launois, T. (2013). Strong similarities between nighttime deposition velocities of carbonyl sulphide and molecular hydrogen inferred from semi-continuous atmospheric observations in Gif-sur-Yvette, Paris region. TELLUS B, 65.

Berkelhammer, M., Asaf, D., Still, C., Montzka, S., Noone, D., Gupta, M., Yakir, D. (2014). Constraining surface carbon fluxes using in situ measurements of carbonyl sulfide and carbon dioxide. GLOBAL BIOGEOCHEM CY, 28(2), 161-179.

Berry J., Wolf A., Campbell J. E., Baker I., Blake N., Blake D., Zhu, Z., A coupled model of the global cycles of carbonyl sulfide and CO2: A possible new window on the carbon cycle. J GEOPHYS RES-BIOGEO, 118(2), 842-852, 2013

Bousquet, P., Ringeval, B., Pison, I., Dlugokencky, E. J., Brunke, E. G., Carouge, C., Ciais, P. (2011). Source attribution of the changes in atmospheric methane for 2006–2008. ATMOS CHEM PHYS,11(8), 3689-3700.

Campbell J. E., Carmichael G. R., Chai T., Mena-Carrasco M., Tang Y., Blake D. R., Stanier C. O., Photosynthetic control of atmospheric carbonyl sulfide during the growing season. SCIENCE, 322(5904), 1085-1088, 2008

Carouge, C., Bousquet, P., Peylin, P., Rayner, P. J., Ciais, P. (2010a). What can we learn from European continuous atmospheric CO 2 measurements to quantify regional fluxes–Part 1: Potential of the 2001 network. ATMOS CHEM PHYS, 10(6), 3107-3117.

Carouge, C., Rayner, P. J., Peylin, P., Bousquet, P., Chevallier, F., Ciais, P. (2010b). What can we learn from European continuous atmospheric CO2 measurements to quantify regional fluxes–Part 2: Sensitivity of flux accuracy to inverse setup. ATMOS CHEM PHYS, 10(6), 3119-3129.

Chevallier, F., Feng, L., Bösch, H., Palmer, P. I., Rayner, P. J. (2010). On the impact of transport model errors for the estimation of CO2 surface fluxes from GOSAT observations. GEOPHYS RES LETT , 37(21).

Chin, M., Davis, D. D. (1993a). Global sources and sinks of OCS and CS2 and their distributions. GLOBAL BIOGEOCHEM CY, 7(2), 321-337.

Chin M., Davis D. D., A reanalysis of carbonyl sulfide as a source of stratospheric background sulfur aerosol. J GEOPHYS RES-OC ATMOS (1984–2012), 100(D5), 8993-9005, 1993b

Chin M., Rood R. B., Lin S. J., Müller J. F., Thompson A. M., Atmospheric sulfur cycle simulated in the global model GOCART: Model description and global properties. J GEOPHYS RES-OC ATMOS (1984–2012), 105(D20), 24671-24687, 2000

Ciais, P., Reichstein, M., Viovy, N., Granier, A., Ogée, J., Allard, V., Valentini, R. (2005). Europe-wide reduction in primary productivity caused by the heat and drought in 2003. NATURE, 437(7058), 529-533.

1 Constant, P., Chowdhury, S. P., Pratscher, J., Conrad, R. (2010). Streptomycetes contributing to atmospheric molecular hydrogen soil uptake are widespread and encode a
2 putative high-affinity [NiFe]-hydrogenase. ENVIRON MICROBIOL, 12(3), 821-829.

3 Conway, T. J., Tans, P. P., Waterman, L. S., Thoning, K. W., Kitzis, D. R., Masarie, K. A., Zhang, N. (1994). Evidence for interannual variability of the carbon cycle from the
4 National Oceanic and Atmospheric Administration/Climate Monitoring and Diagnostics Laboratory global air sampling network. J GEOPHYS RES - ATMOS (1984–
5 2012), 99(D11), 22831-22855.

6 Geng, C., Mu, Y. (2006). Carbonyl sulfide and dimethyl sulfide exchange between trees and the atmosphere. ATMOS ENVIRON, 40(7), 1373-1383.

7 Grace, J., Rayment, M. (2000). Respiration in the balance. NATURE, 404(6780), 819-820.

8 Hauglustaine, D. A., Brasseur, G. P., Walters, S., Rasch, P. J., Müller, J. F., Emmons, L. K., Carroll, M. A. (1998). MOZART, a global chemical transport model for ozone
9 and related chemical tracers: 2. Model results and evaluation. J GEOPHYS RES – ATMOS (1984–2012), 103(D21), 28291-28335.

10 Hourdin, F., Musat, I., Bony, S., Braconnot, P., Codron, F., Dufresne, J. L., Lott, F. (2006). The LMDZ4 general circulation model: climate performance and sensitivity to
11 parametrized physics with emphasis on tropical convection. CLIM DYNAM, 27(7-8), 787-813.

12 Kato, H., Saito, M., Nagahata, Y., Katayama, Y. (2008). Degradation of ambient carbonyl sulfide by Mycobacterium spp. in soil. MICROBIOLOGY+, 154(1), 249-255.

13 Kesselmeier, J., Teusch, N., Kuhn, U. (1999). Controlling variables for the uptake of atmospheric carbonyl sulfide by soil. J GEOPHYS RES – ATMOS (1984–
14 2012), 104(D9), 11577-11584.

15 Kettle, A. J., Kuhn, U., Von Hobe, M., Kesselmeier, J., Andreae, M. O. (2002). Global budget of atmospheric carbonyl sulfide: Temporal and spatial variations of the
16 dominant sources and sinks. J GEOPHYS RES - ATMOS (1984–2012), 107(D22), ACH-25.

17

18 Kloster S., Feichter J., Maier-Reimer E., Six K. D., Stier P., Wetzel P., DMS cycle in the marine ocean-atmosphere system: a global model study. BIOGEOSCIENCES, 3(1),
19 29-51, 2006

Knohl, A., Werner, R. A., Brand, W. A., Buchmann, N. (2005). Short-term variations in $\delta^{13}C$ of ecosystem respiration reveals link between assimilation and respiration in a deciduous forest. OECOLOGIA, 142(1), 70-82.

Koch D., Jacob D., Tegen I., Rind D., Chin M., Tropospheric sulfur simulation and sulfate direct radiative forcing in the Goddard Institute for Space Studies general circulation model. J GEOPHYS RES-OC ATMOS (1984–2012), 104(D19), 23799-23822, 1999

Kottek, M., Grieser, J., Beck, C., Rudolf, B., Rubel, F. (2006). World map of the Köppen-Geiger climate classification updated. METEOROL Z,15(3), 259-263.

Krinner, G., Viovy, N., de Noblet-Ducoudré, N., Ogée, J., Polcher, J., Friedlingstein, P., Prentice, I. C. (2005). A dynamic global vegetation model for studies of the coupled atmosphere-biosphere system. GLOBAL BIOGEOCHEM CY, 19(1).

Kobayashi, K., Salam, M. U. (2000). Comparing simulated and measured values using mean squared deviation and its components. AGRON J, 92(2), 345-352.

Kuppel, S., Peylin, P., Maignan, F., Chevallier, F., Kiely, G., Montagnani, L., Cescatti, A. (2014). Model–data fusion across ecosystems: from multi-site optimizations to global simulations.

Lasslop, G., Reichstein, M., Papale, D., Richardson, A. D., Arneth, A., Barr, A., Wohlfahrt, G. (2010). Separation of net ecosystem exchange into assimilation and respiration using a light response curve approach: critical issues and global evaluation. GLOB CHANGE BIOL, 16(1), 187-208.

Launois T., Belviso S., Bopp L., Fichot C.G. and Peylin P., A new model for the global biogeochemical cycle of carbonyl sulfide. Part 1: Assessment of direct marine emissions with an oceanic general circulation and biogeochemistry model, in press. (ACPD, 2014)

Locatelli, R., Bousquet, P., Chevallier, F., Fortems-Cheney, A., Szopa, S., Saunois, M., Wilson, C. (2013). Impact of transport model errors on the global and regional methane emissions estimated by inverse modelling. ATMOS CHEM PHYS, 13(19), 9917-9937.

Lorimer, G. H., Pierce, J. (1989). Carbonyl sulfide: an alternate substrate for but not an activator of ribulose-1, 5-bisphosphate carboxylase. J BIOL CHEM, 264(5), 2764-2772.

Marland, G., Brenkert, A., Olivier, J. (1999). CO_2 from fossil fuel burning: a comparison of ORNL and EDGAR estimates of national emissions. ENVIRON SCI POLICY, 2(3), 265-273.

Masotti, I., Belviso, S., Bopp, L., Tagliabue, A., Bucciarelli, E. Effects of light and phosphorus on summer DMS dynamics in subtropical waters using a global ocean biogeochemical model. Environ. Chem., in press.

1

2

3 Maseyk, K., Berry, J. A., Billesbach, D., Campbell, J. E., Torn, M. S., Zahniser, M., Seibt, U. (2014). Sources and sinks of carbonyl sulfide in an agricultural field in the
4 Southern Great Plains. P NATL ACAD SCI USA, 111(25), 9064-9069.

5 Montzka, S., Tans, P. (2004, December). Can Carbonyl Sulfide Help Constrain Gross Vegetative Fluxes of Carbon Dioxide?, AGU Fall Meeting Abstracts (Vol. 1, p. 04).

6 Montzka S. A., Calvert P., Hall B. D., Elkins J. W., Conway T. J., Tans P. P., Sweeney, C., On the global distribution, seasonality, and budget of atmospheric carbonyl sulfide
7 (COS) and some similarities to CO2. J GEOPHYS RES-OC ATMOS (1984–2012), 112(D9), 2007

8 Morfopoulos, C., Foster, P. N., Friedlingstein, P., Bousquet, P., Prentice, I. C. (2012). A global model for the uptake of atmospheric hydrogen by soils. GLOBAL
9 BIOGEOCHEM CY, 26(3).

10 Nguyen, B. C., Mihalopoulos, N., Putaud, J. P., Bonsang, B. (1995). Carbonyl sulfide emissions from biomass burning in the tropics. J ATMOS CHEM, 22(1-2), 55-65.

11 T.Ogawa, K.Noguchi, M. Saito, Y.Nagahata, H. Kato, A. Ohtaki, H.Nakayama, N.Dohmae, Y.Matsushita, M.Odaka, M.Yohda, H. Nyunoya and Y. Katayama (2013).
12 Carbonyl Sulfide hydrolase from Thiobacillus thioparus Strain THI115 is one of the β‑Carbonic Anhydrase family enzymes. J. Am. Chem. Soc., 135, 3818−3825,
13 doi.:10.1021/ja307735e |

14 Patra, P. K., Houweling, S., Krol, M., Bousquet, P., Belikov, D., Bergmann, D., Wilson, C. (2011). TransCom model simulations of CH 4 and related species: linking
15 transport, surface flux and chemical loss with CH4 variability in the troposphere and lower stratosphere. ATMOS CHEM PHYS, 11(24), 12813-12837.

16 **Peylin P.,** P. Rayner, P. Bousquet, C. Carouge, F. Hourdin, P. Heinrich, P. Ciais, and AEROCARB contributors, Daily CO2 flux over Europe from continuous atmospheric
17 measurements: 1, inverse methodology, **Atmos. Chem. and Phys.**, 5, 3173-3186, ISI:000233610300001, 2005.

18 Peylin, P., Bacour, C., MacBean, N., Leonard, S., Maignan, F., Thum, T., Santaren, D. (2014, May). How best to optimize a global process-based carbon land surface model?
19 EGU General Assembly Conference Abstracts (Vol. 16, p. 10302).

20 Piovesan, G., & Adams, J. M. (2000). Carbon balance gradient in European forests: interpreting EUROFLUX. J VEG SCI, 11(6), 923-926.

1 Poulter, B., Ciais, P., Hodson, E., Lischke, H., Maignan, F., Plummer, S., Zimmermann, N. E. (2011). Plant functional type mapping for earth system models. GEOSCI
2 MODEL DEV, 4(4), 993-1010.

3 Poulter, B., Frank, D., Ciais, P., Myneni, R. B., Andela, N., Bi, J., Van der Werf, G. R. (2014). Contribution of semi-arid ecosystems to interannual variability of the global
4 carbon cycle. NATURE, 509(7502), 600-603.

5 Protoschill-Krebs, G., Kesselmeier, J. (1992). Enzymatic Pathways for the Consumption of Carbonyl Sulphide (COS) by Higher Plants BOT ACTA,105(3), 206-212.

6 Protoschill-Krebs, G., Wilhelm, C., Kesselmeier, J. (1995). Consumption of carbonyl sulphide by Chlamydomonas reinhardtii with different activities of carbonic anhydrase
7 (CA) induced by different CO2 growing regimes. BOT ACTA, 108(5), 445-448.

8 Protoschill-Krebs, G., Wilhelm, C., Kesselmeier, J. (1996). Consumption of carbonyl sulphide (COS) by higher plant carbonic anhydrase (CA). ATMOS ENVIRON, 30(18),
9 3151-3156.

10 Reichstein, M., Falge, E., Baldocchi, D., Papale, D., Aubinet, M., Berbigier, P., Valentini, R. (2005). On the separation of net ecosystem exchange into assimilation and
11 ecosystem respiration: review and improved algorithm. GLOB CHANGE BIOL, 11(9), 1424-1439.

12 Sandoval-Soto, L., Stanimirov, M., Hobe, M. V., Schmitt, V., Valdes, J., Wild, A., Kesselmeier, J. (2005). Global uptake of carbonyl sulfide (COS) by terrestrial vegetation:
13 Estimates corrected by deposition velocities normalized to the uptake of carbon dioxide (CO 2). BIOGEOSCIENCES, 2(2), 125-132.

14 Sandoval-Soto, L., Kesselmeier, M., Schmitt, V., Wild, A., Kesselmeier, J. (2012). Observations of the uptake of carbonyl sulfide (COS) by trees under elevated atmospheric
15 carbon dioxide concentrations. Biogeosciences Discussions, 9(2), 2123-2152.

16 Scartazza, A., Mata, C., Matteucci, G., Yakir, D., Moscatello, S., Brugnoli, E. (2004). Comparisons of δ13C of photosynthetic products and ecosystem respiratory CO2 and
17 their responses to seasonal climate variability. OECOLOGIA,140(2), 340-351.

18 Schaphoff, S., Lucht, W., Gerten, D., Sitch, S., Cramer, W., Prentice, I. C. (2006). Terrestrial biosphere carbon storage under alternative climate projections. CLIMATIC
19 CHANGE, 74(1-3), 97-122.

1 Schenk, S., Kesselmeier, J., Anders, E. (2004). How does the exchange of one oxygen atom with sulfur affect the catalytic cycle of carbonic anhydrase? CHEM-EUR
2 J, 10(12), 3091-3105.

3 Scherr, N., Nguyen, L. (2009). Mycobacterium versus Streptomyces—we are different, we are the same. CURR OPIN MICROBIOL, 12(6), 699-707.

4 Seibt, U., Wingate, L., Lloyd, J., Berry, J. A. (2006). Diurnally variable $\delta 18O$ signatures of soil CO_2 fluxes indicate carbonic anhydrase activity in a forest soilJ GEOPHYS
5 RES - BIOGEO(2005–2012), 111(G4).

6 Seibt, U., Kesselmeier, J., Sandoval-Soto, L., Kuhn, U., Berry, J. A. (2010). A kinetic analysis of leaf uptake of COS and its relation to transpiration, photosynthesis and
7 carbon isotope fractionation. BIOGEOSCIENCES, 7(1), 333-341.

8

9 Simmons, J. S., Klemedtsson, L., Hultberg, H., Hines, M. E. (1999). Consumption of atmospheric carbonyl sulfide by coniferous boreal forest soils. J GEOPHYS RES -
10 ATMOS (1984–2012), 104(D9), 11569-11576.

11 Sitch, S., Smith, B., Prentice, I. C., Arneth, A., Bondeau, A., Cramer, W., Venevsky, S. (2003). Evaluation of ecosystem dynamics, plant geography and terrestrial carbon
12 cycling in the LPJ dynamic global vegetation model. GLOB CHANGE BIOL, 9(2), 161-185.

13 Smith-Downey, N. V., Randerson, J. T., Eiler, J. M. (2006). Temperature and moisture dependence of soil H2 uptake measured in the laboratory. GEOPHYS RES
14 LETT, 33(14).

15 Stimler, K., Montzka, S. A., Berry, J. A., Rudich, Y., Yakir, D. (2010). Relationships between carbonyl sulfide (COS) and CO_2 during leaf gas exchange. NEW
16 PHYTOL, 186(4), 869-878.

17 Suntharalingam P., Kettle A. J., Montzka S. M., Jacob D. J., Global 3-D model analysis of the seasonal cycle of atmospheric carbonyl sulfide: Implications for terrestrial
18 vegetation uptake. GEOPHYS RES LETT, 35(19), 2008

19 Tarantola, A. (1987). Inverse problems theory. Methods for Data Fitting and Model Parameter Estimation. Elsevier, Southampton.

20 Takahashi, T., Sutherland, S. C., Wanninkhof, R., Sweeney, C., Feely, R. A., Chipman, D. W., De Baar, H. J., Climatological mean and decadal change in surface ocean
21 pCO2, and net sea–air CO_2 flux over the global oceans, Deep Sea Research Part II: Topical Studies in Oceanography 56.8 (2009): 554-577.

1 Thornton, P. E., Lamarque, J.-F., Rosenbloom, N. A., and Mahowald, N. M.: Influence of carbon-nitrogen cycle coupling on land model response to CO_2 fertilization and
2 cliate variability, GLOBAL BIOGEOCHEM CY, 21, 1-15, 2007.

3 Van der Werf, G. R., Randerson, J. T., Giglio, L., Collatz, G. J., Mu, M., Kasibhatla, P. S., Van Leeuwen, T. T., Global fire emissions and the contribution of deforestation,
4 savanna, forest, agricultural, and peat fires (1997–2009), ATMOS CHEM PHYS 10.23 (2010): 11707-11735.

5 Van Diest, H., and J. Kesselmeier. Soil atmosphere exchange of carbonyl sulfide (COS) regulated by diffusivity depending on water-filled pore space. BIOGEOSCIENCES,
6 5.2 (2008): 475-483.

7 Wania, R., Ross, I., Prentice, I. C. (2010). Implementation and evaluation of a new methane model within a dynamic global vegetation model: LPJ-WHyMe v1. 3.1, GEOSCI
8 MODEL DEV, 3, 565–584, doi: 10.5194.

9 Whelan, M. E., Min, D. H., Rhew, R. C. (2013). Salt marsh vegetation as a carbonyl sulfide (COS) source to the atmosphere. ATMOS ENVIRON, 73, 131-137.

10 White, M. L., Zhou, Y., Russo, R. S., Mao, H., Talbot, R., Varner, R. K., Sive, B. C. (2011). Carbonyl sulfide exchange in a temperate loblolly pine forest grown under
11 ambient and elevated CO2, ATMOS CHEM PHYS, 10, 547–561, 2010

12 Wingate, Lisa, Seibt, U., Maseyk, K., OgEE, J., Almeida, P., Yakir, D., Mencuccini, M., Evaporation and carbonic anhydrase activity recorded in oxygen isotope signatures
13 of net CO2 fluxes from a Mediterranean soil, GLOB CHANGE BIOL 14.9 (2008): 2178-2193.

14 Wingate, Lisa, Ogée, J., Burlett, R., Bosc, A., Devaux, M., Grace, J., Gessler, A., Photosynthetic carbon isotope discrimination and its relationship to the carbon isotope
15 signals of stem, soil and ecosystem respiration, NEW PHYTOL 188.2 (2010): 576-589.

16 Wöhlfahrt G., Brilli F., Hörtnagl L., Xu X., Bingemer H., Hansel A., Loreto F., Carbonyl sulfide (COS) as a tracer for canopy photosynthesis, transpiration and stomatal
17 conductance: potential and limitations†. PLANT CELL ENVIRON, 35(4), 657-667, 2012

18 Xu X., Bingemer H. G., Georgii H. W., Schmidt U., Bartell, U., Measurements of carbonyl sulfide (COS) in surface seawater and marine air, and estimates of the air-sea flux
19 from observations during two Atlantic cruises. J GEOPHYS RES-OC ATMOS (1984–2012), 106(D4), 3491-3502, 2001

20 Yi, Zhigang Wang, X., Sheng, G., Zhang, D., Zhou, G., & Fu, J., Soil uptake of carbonyl sulfide in subtropical forests with different successional stages in south China, J
21 GEOPHYS RES: Atmospheres (1984–2012) 112.D8 (2007).

22

1

2

3

4

5

6

7

8

9

10

11   Table 1: Summary of forward and inverse simulations performed using the LMDz transport model and specific setups of surface fluxes. We compared three dynamic global vegetation models

12   (DGVMs), carried out a series of sensitivity tests and optimized major fluxes (the allowed range of variations is expressed in %). ORC stands for ORCHIDEE. CLM4CN stands for NCAR-

13   CLM4. LPJ stands for… v_{H2} and v_{OCS} are the deposition velocities of H_2 and OCS.

		Simulations names	OCS leaf uptake[1]	OCS uptake by oxic soil[2]	OCS oceanic emissions
FORWARD RUNS	MODEL INTER-COMPARISON	STD_ORC	GPP from ORC	v_{H2} map (Morfopoulos et al. , 2012)	Direct: Launois et al.(2014)
				$v_{OCS}/v_{H2} = 0.75$	Indirect from DMS: Masotti et al. (in press)
					Indirect from CS_2: Kettle et al. (2002)
		STD_CLM4CN	GPP from CLM4CN	"	"
		STD_LPJ	GPP from LPJ	"	"

35

SENSITIVITY TESTS	TEST_Ocean_±30	GPP from ORC	"	Increased/Decreased by 30%
	TEST_Soil_MORF_0.5:1	"	ν_{H2} map (Morfopoulos et al. , 2012) $\nu_{OCS}/\nu_{H2} = 0.5$ (H. Chen pers. com.)	Direct: Launois et al.(2014) Indirect from DMS: Masotti et al. (in press) Indirect from CS_2: Kettle et al. (2002)
	TEST_Soil_MORF_1:1	"	ν_{H2} map (Morfopoulos et al. , 2012) $\nu_{OCS}/\nu_{H2} = 1$ (Belviso et al., 2013)	"
	TEST_Soil_BOUSQ_0.5:1	"	ν_{H2} map (Bousquet et al. , 2011) $\nu_{OCS}/\nu_{H2} = 0.5$ (H. Chen pers. com.)	"
	TEST_Soil_BOUSQ_1:1		ν_{H2} map (Bousquet et al. , 2011) $\nu_{OCS}/\nu_{H2} = 1$ (Belviso et al., 2013)	"
OPTIMIZATION	OPTIM_H-Er	±50%	±50%	-30 / +50%
	OPTIM_L-Er	±10%	±10%	±10%
	OPTIM_LEAF_ONLY	±50%	±10%	±10%
	OPTIM_SOIL_ONLY	±10%	±50%	±10%
	OPTIM_OCEAN_ONLY	±10%	±10%	-30 / +50%

1   [1] LRUs from Seibt et al. (2010) are used in all simulations, sensitivity tests and optimizations.

2   [2] Note that the OCS emissions by anoxic soils were kept unchanged between the simulations, and attributed a ±30% variation range in all optimization configurations.

3   All other surface fluxes are either described in the method section or taken directly from Kettle et al. (2002). They are attributed a ±10% variation range in all optimization configurations.

4

5

6

1

2

3

4

5

6

7

8

9

10

11

12

13

14 Table 2: Overview of global budgets of carbonyl sulfide. Units are Gg S yr^{-1}. Shaded cells include new estimates which are compared with data from the recent literature. Only fluxes provided

15 by Kettle et al. (2002) and in the present study have been transported using the LMDz model. DGVM stands for dynamic global vegetation models.

	PROCESSES	Kettle et al. (2002)	Montzka et al. (2007)[2]	Suntharalingam et al. (2008)	Berry et al. (2013)	This study		
	DGVM used	not relevant	not relevant	not relevant	SiB3	ORC	LPJ	CLM4CN
SINKS	Plant uptake	-238	-1115	-490	-738	-1335	-1069	-930

Soil uptake (oxic soils)	-130	-130	-130	-355		-510	
Destruction by OH radicals	-120	-120	-120	-101		-100	
Total sinks	**-488**	**-1365**	**-740**	**-1194**	**-1945**	**-1679**	**-1540**
Anoxic soils and wetlands	26	26	26	neglected		101	
Direct oceanic emissions of OCS	39	39		639[3]		813	
Indirect oceanic emissions of OCS (from DMS)	156	156	230	156		133	
Indirect oceanic emissions of OCS (from CS_2)	81	81		81*		81	
Direct anthropogenic emissions of OCS	64	64		64*		64	
Indirect anthropogenic emissions of OCS (from DMS and CS_2)	116	116	180	116		116	
Biomass burning	38	106	70[1]	136[4]		70	
Total sources	**552**	**588**	**506**	**1192**		**1379**	
Net total	**64**	**-776**	**-234**	**1**	**-566**	**-300**	**-161**

1 [1]Modification to Kettle et al. (2002): biomass burning data are from the total flux of Nguyen et al. (1995).

2 [2]Median fluxes taken from Montzka et al. (2007) as (max.- min.)/2.

3 [3] To provide a balanced global budget of OCS, Berry et al. (2013) increased the marine emissions of Kettle et al. (2002) by 600 Gg S yr^{-1}.

4 [4]An upper estimate supposedly taken from Kettle et al. (2002) and consistent with the new estimates of Montzka et al. (2007).

5 *As proposed by Kettle et al. (2002) but incorrectly reported in Table 1 of Berry et al. (2013).

6

Table 3: OCS surface fluxes before and after their optimization. Units are Gg S yr^{-1}. DGVM stands for dynamic global vegetation models. All allowed ranges of variation presented here correspond to the "H-Er" case (Table 1).

	PROCESSES	Before optimization upper and lower limits of variation			After optimization Adjusted fluxes		
	DGVM	ORC	LPJ	CLM4CN	ORC	LPJ	CLM4CN
SINKS	Plant uptake	[-2003 , -668]	[-1604 , -.535]	[-1395 , -465]	-708	-663	-772
	Soil uptake (oxic soils)	[-770 , -255]			-283	-398	-507
	Destruction by OH radicals	[-110 , -90]			-110*	-104	-110*
	Total sinks	[-2883 , -1013]	[-2484 , -880]	[-2275 , -810]	**-1101**	**-1165**	**-1389**
SOURCES	Anoxic soils and wetlands	[50 , 150]			50*	50*	50*
	Direct oceanic emissions of OCS	[569 , 1220]			610*	659	805
	Indirect oceanic emissions of OCS (from DMS)	[93 , 173]			93*	104	173*
	Indirect oceanic emissions of OCS (from CS$_2$)	[57 , 105]			105*	105*	105*
	Direct anthropogenic emissions of OCS	[58 , 70]			58*	58*	58*
	Indirect anthropogenic emissions of OCS (from DMS and CS$_2$)	[104 , 128]			104*	104*	104*
	Biomass burning	[63 , 77]			71	74	74
	Total sources	[994 , 1923]			**1091**	**1154**	**1369**
	Net total	[-1889 , 910]	[-1490 , 1043]	[-1281 , 1113]	**-10**	**-1**	**-20**

1   *Surface fluxes which, after optimization, have reached the set upper or lower limits of variation.

2   Computed plant and soil uptakes after optimization are in average 714 and 396 GgS yr-1, respectively.

1
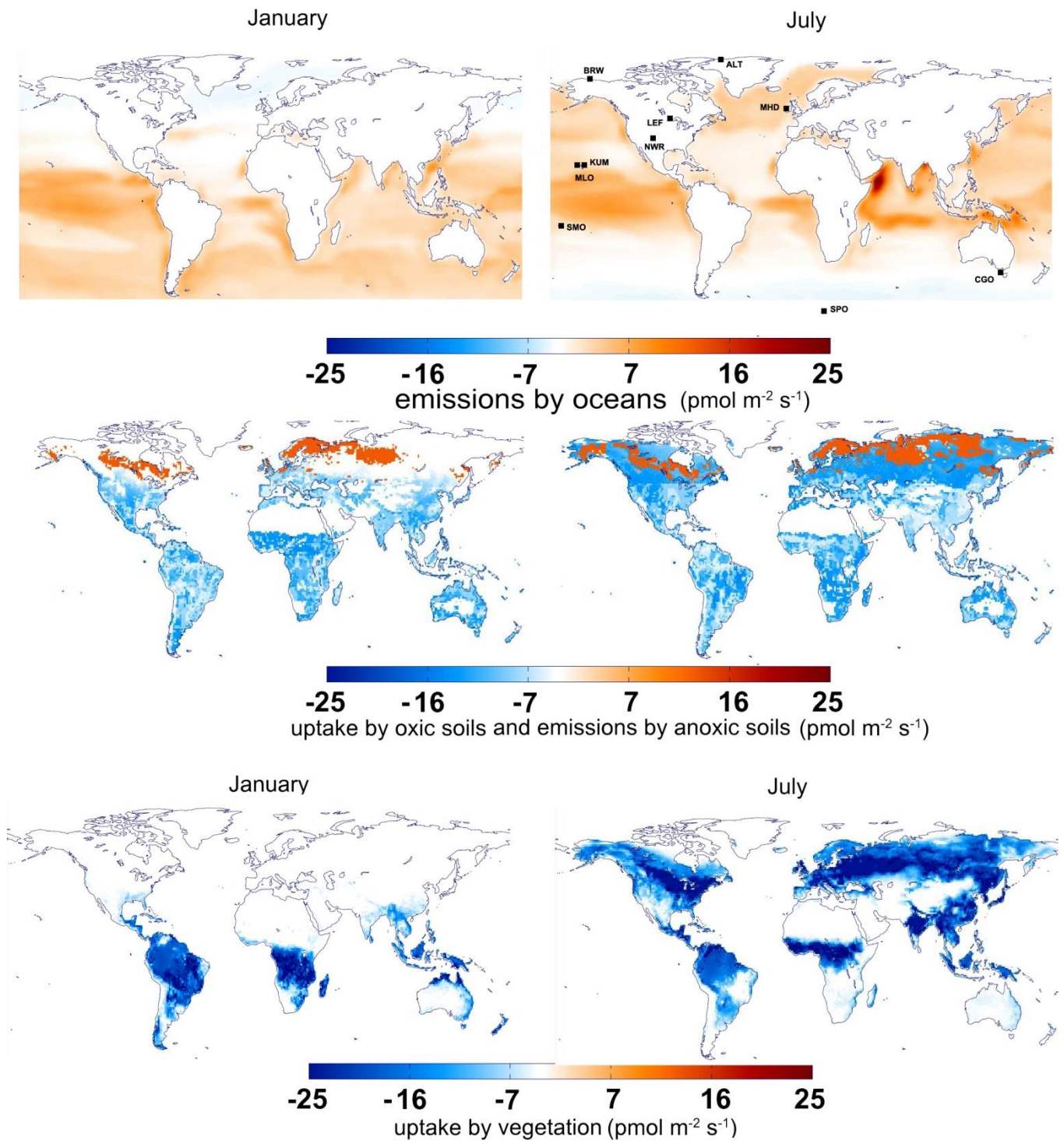
Figure 1: Monthly mean direct oceanic emissions (first row, from the standard run of Launois et al. (2014))
for January (left column) and July (right column), monthly mean uptake of OCS by soils (second row, using
H_2 deposition velocities (Morfopoulos et al., 2012) and OCS vs. H_2 deposition velocities in a 0.75:1 ratio)
and vegetation (third row, deduced from the GPP of ORC). The 10 NOAA stations are: SPO, South Pole,
89.9°S, 59°E; CGO, Cape Grim, Australia, 40.7°S, 144.8°E; SMO, American Samoa, 14.3°S, 170.6°W;
MLO, Mauna Loa, United States, 19.5°N, 155.6°W; NWR, Niwot Ridge, United States, 40.1°N, 105.6°W;
BRW, Barrow, United States, 71.3°N, 156.6°W; ALT, Alert, Canada, 82.5°N, 62.3°W; MHD, Mace Head,

Ireland, 53°N, 10°W; KUM, Cape Kumukahi, Hawaii, United States, 19.5°N, 154.8°W and LEF, Wisconsin, United States, 45.6°N,90.2°W.
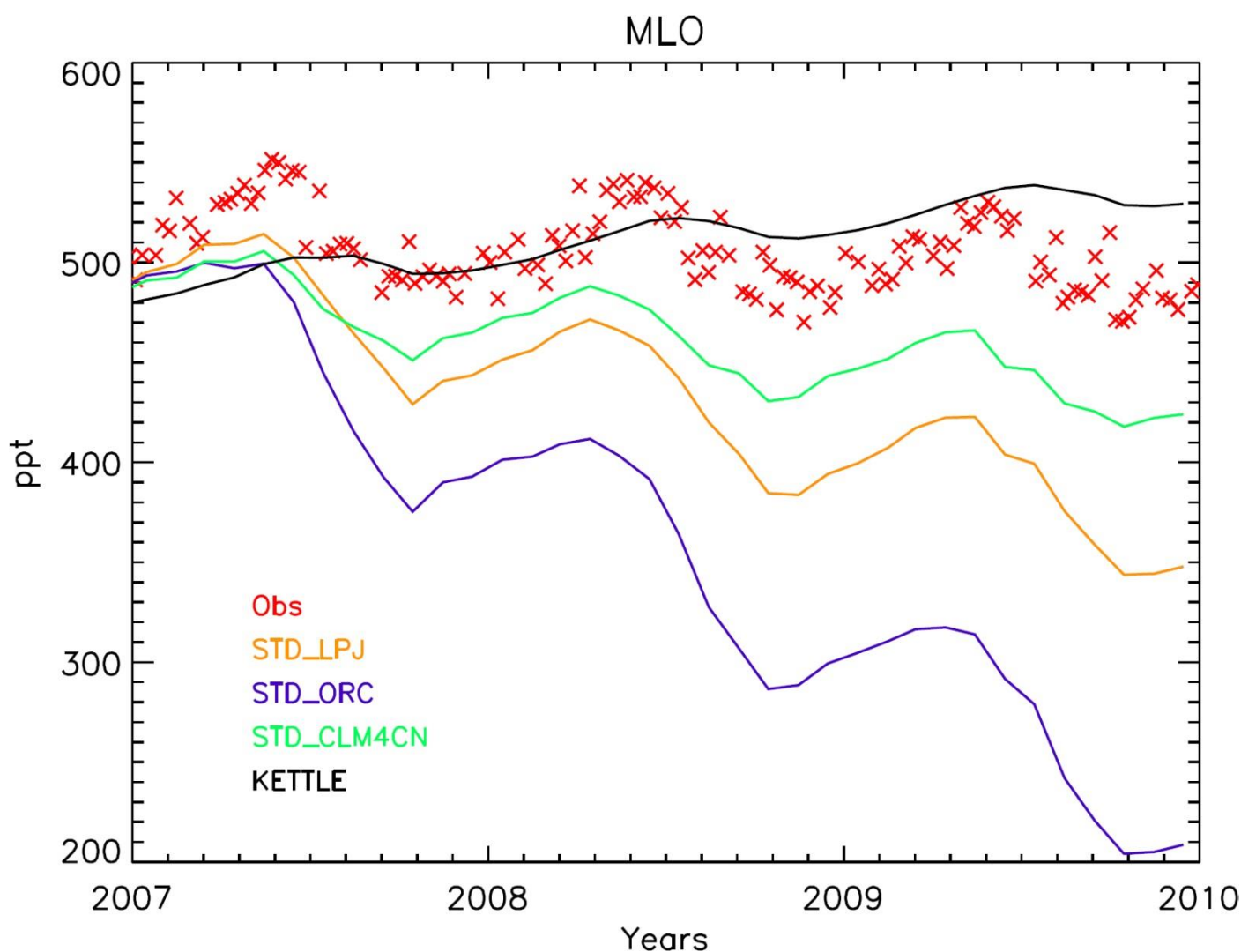
Figure 2: Annual variations of OCS monthly mean mixing ratios (in ppt), simulated and monitored at Mauna Loa. Simulations with the LMDz model use the "STD_ORC", "STD_LPJ" and "STD_CLM4CN" configurations described in Table 1. Data derived solely from the Kettle et al. (2002) surface fluxes are shown in black solid line. Observations (red crosses) are from NOAA-ESRL global monitoring network (Montzka et al., 2007).
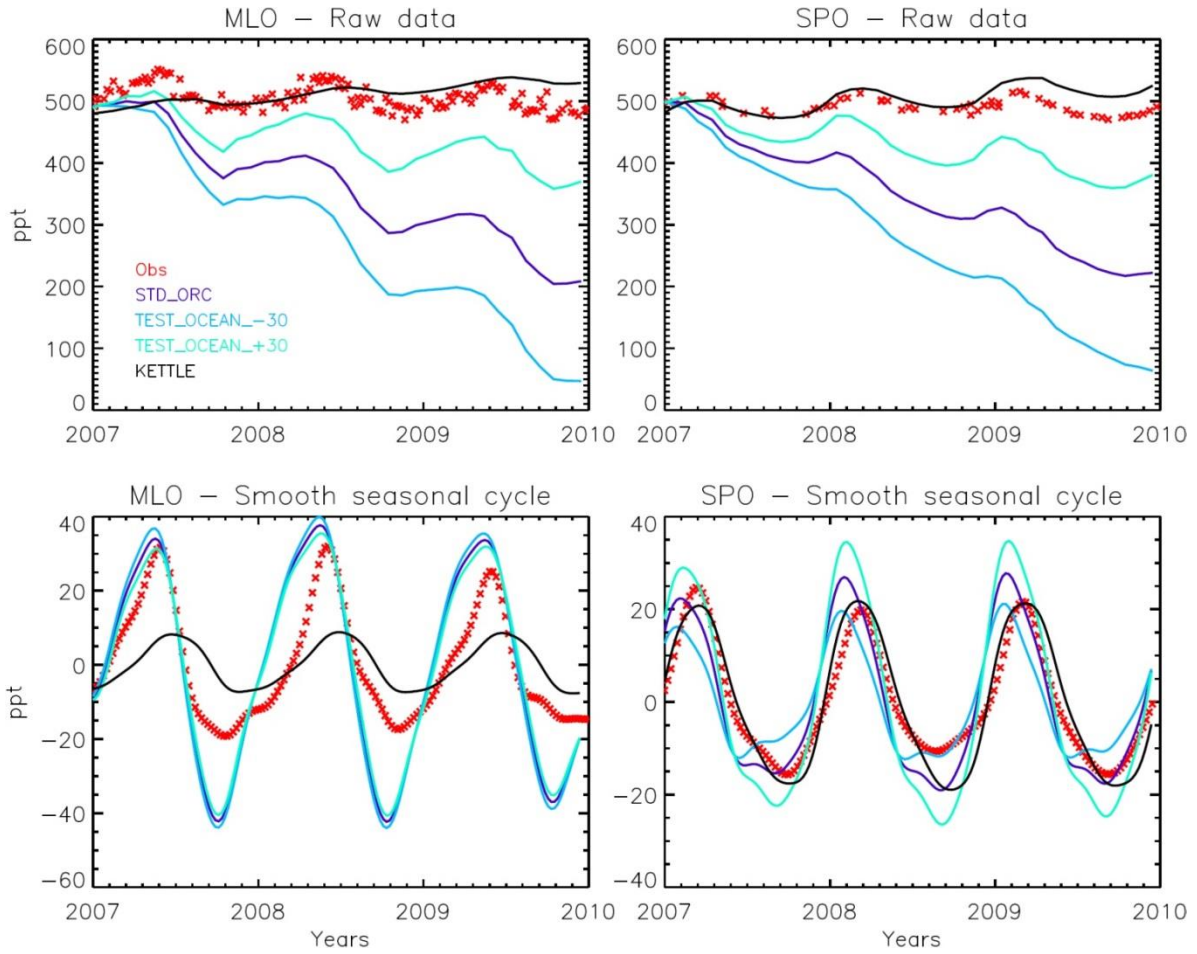
Figure 3: Sensitivity tests performed using the "TEST_Ocean_±30" setup of surface fluxes (Table 1) to simulate the annual variations of OCS monthly mean mixing ratios (upper panels) simulated and monitored at Mauna Loa (left column) and South Pole (right column). Raw data were fitted with a function including a polynomial term (1st order) and four harmonics. The residuals of the functions were further smoothed in the Fourier space, using a low pass filter (cutoff frequency of 65 days) to define a so-called smoothed curve (function plus filtered residuals). The mean seasonal cycle is defined from the smoothed curve after subtraction of the polynomial term. The corresponding smoothed seasonal variations obtained are displayed in lower panels. The simulations based solely on the Kettle et al. (2002) surface fluxes are shown with a black solid line. Observations (red crosses) are from NOAA-ESRL global monitoring network (Montzka et al., 2007).

1

2

3

4
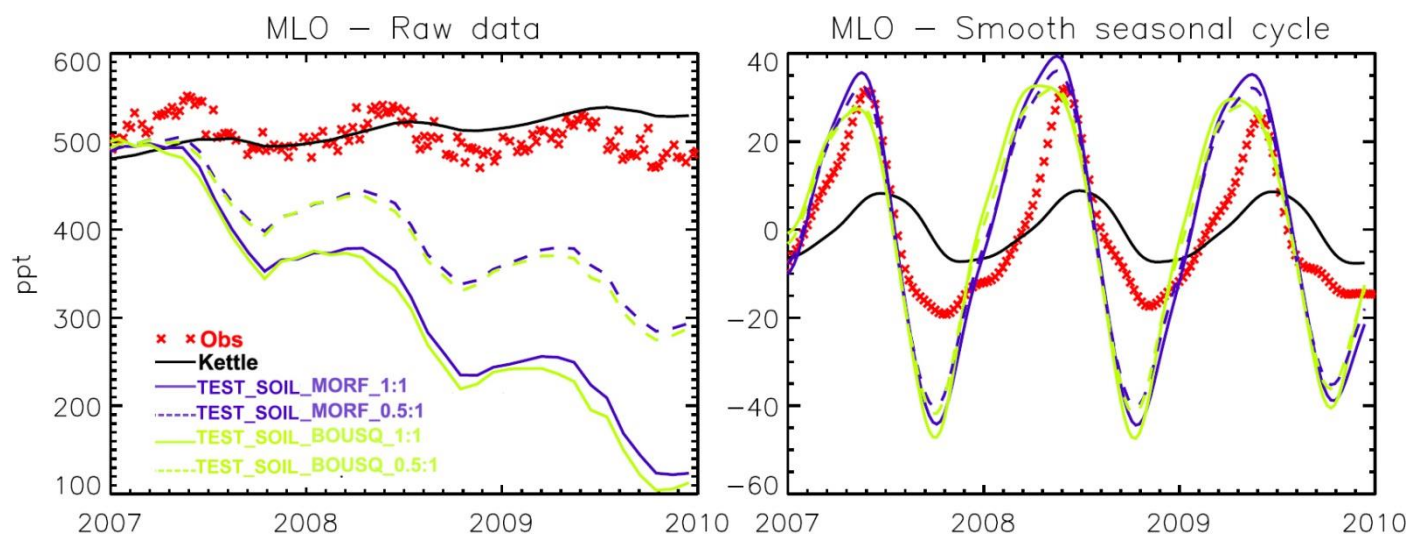
Figure 4: Sensitivity tests performed using the "TEST_Soil_MORF_0.5:1", "TEST_Soil_MORF_1:1", "TEST_Soil_BOUSQ_0.5:1" and "TEST_Soil_BOUSQ_1:1" setups of surface fluxes (Table 1) to simulate annual variations of OCS monthly mean mixing ratios (left panel) and smoothed seasonal variations obtained after removing the annual trends (right panel), at Mauna Loa. The simulations based solely on the Kettle et al. (2002) surface fluxes are shown in black solid line. Observations (red crosses) are from NOAA-ESRL global monitoring network (Montzka et al., 2007).

12

13

14

15

16

17

18

19

20
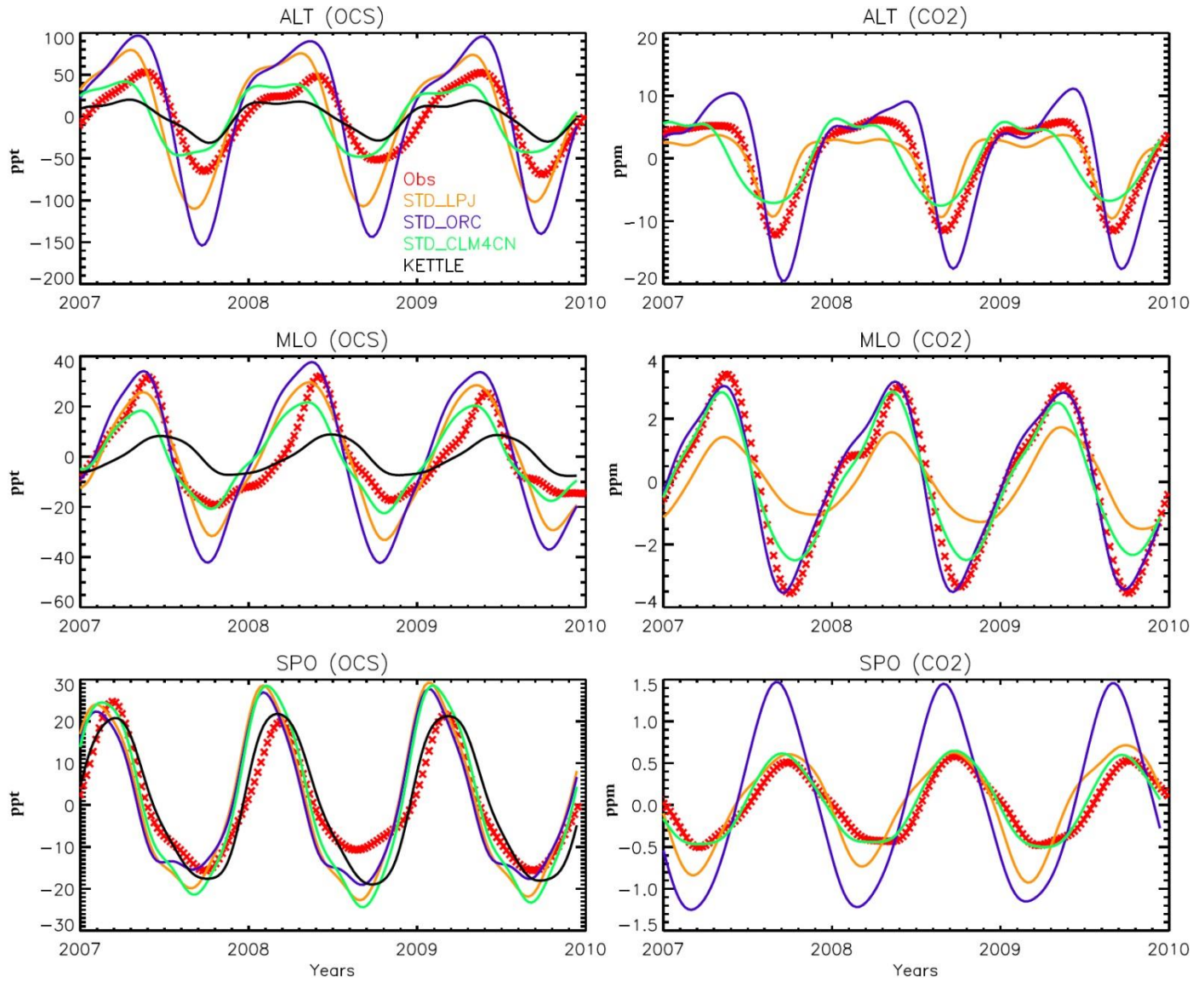
Figure 5: Smoothed seasonal cycles of OCS (left column) and CO_2 (right column) monthly mean mixing ratios, simulated at ALT, MLO and SPO, and obtained after removing the annual trends. Simulations obtained with the LMDz model using the "STD_ORC", "STD_CLM4CN", "STD_LPJ" setups (Table 1). Data derived solely from the Kettle et al. (2002) surface fluxes are shown in black solid line. Observations (red crosses) are from NOAA-ESRL global monitoring network (Montzka et al., 2007).

1
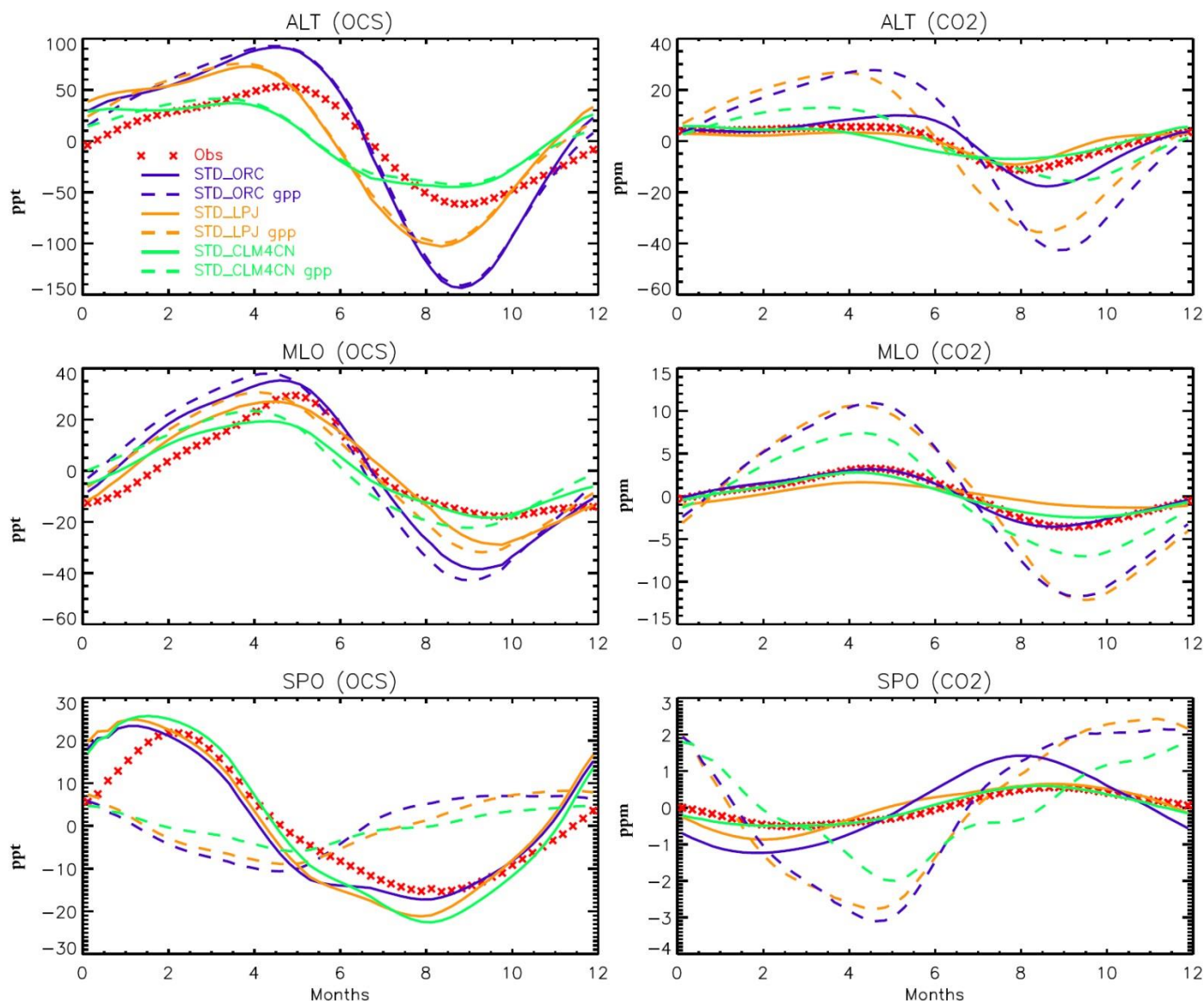
Figure 6: Average smoothed seasonal cycles of OCS (left column) and CO_2 (right column) monthly mean mixing ratios, simulated at ALT, MLO and SPO, and obtained after removing the annual trends. OCS cycles simulated with the LMDz model using the "STD_ORC", "STD_LPJ" and "STD_CLM4CN" setups (Table 1). The dashed lines represent the smoothed seasonal cycles of the OCS (left column) and CO_2 (right column) monthly mean mixing ratios when only the contribution of the leaf OCS uptake (resp. the GPPs) of the three vegetation models are used in the LMDz transport model ("ORC gpp", "CLM4CN gpp" and "LPJ gpp"). Observations (red crosses) are from NOAA-ESRL global monitoring network (Montzka et al., 2007).
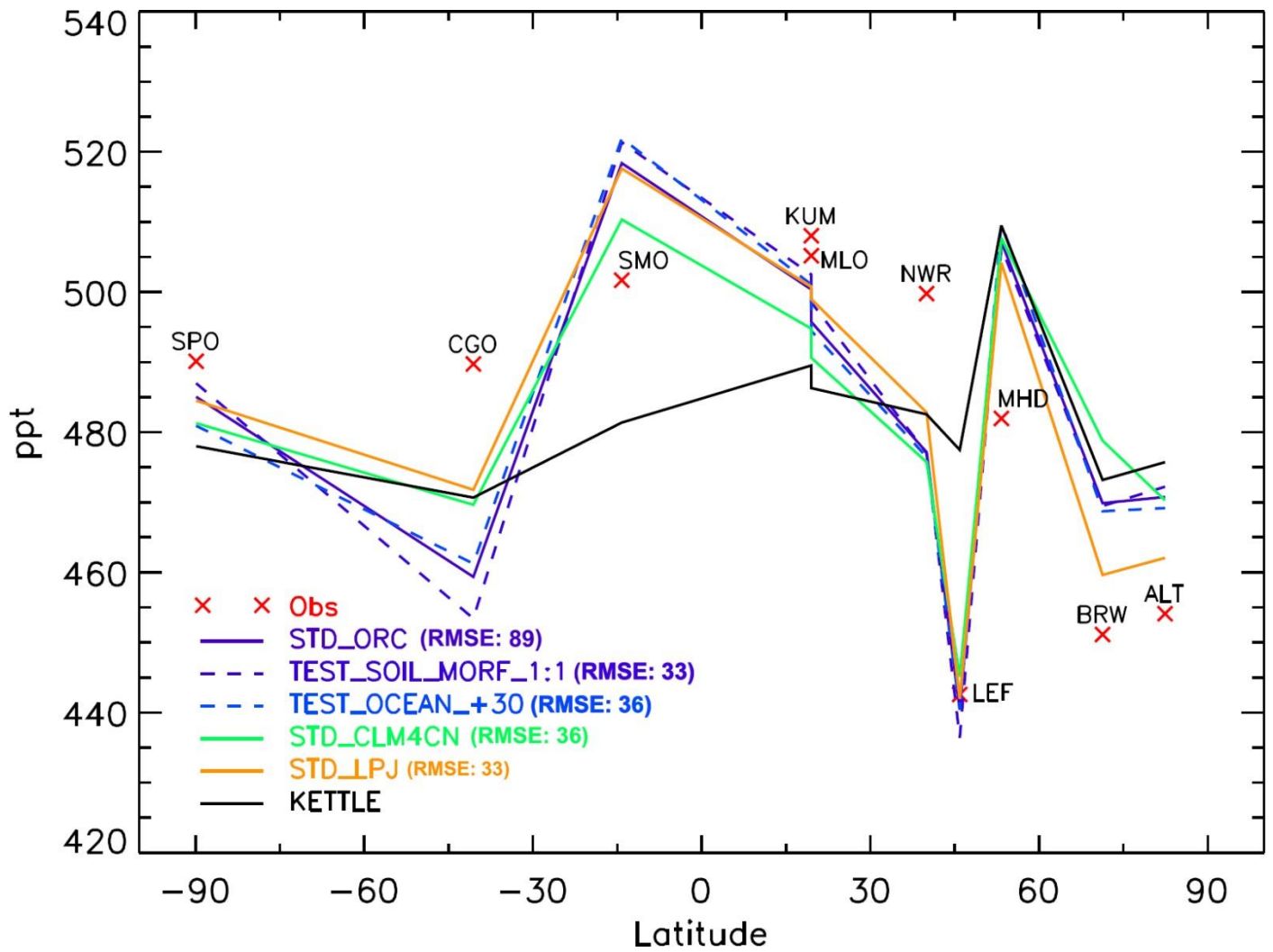
10

11

12

13

1

2

Figure 7: Differences in OCS annual mean mixing ratios between 10 stations of the NOAA monitoring network, plotted as a function of latitude, for observations (red crosses surmounted by station acronyms) and simulations (no symbol). Note that the global mean for each mixing ratio series has been set to the global mean of the observations. Simulations obtained with the LMDz model using the "STD_ORC", "STD_CLM4CN" and "STD_LPJ" setups (Table 1). Data derived solely from the Kettle et al. (2002) surface fluxes are shown in black solid line. The sensitivity of latitudinal gradients to changes in soil uptake and ocean emissions (dashed colored lines) was investigated using the "TEST_Soil_MORF_1:1 +30%" and "TEST_Ocean_+30%" setups.
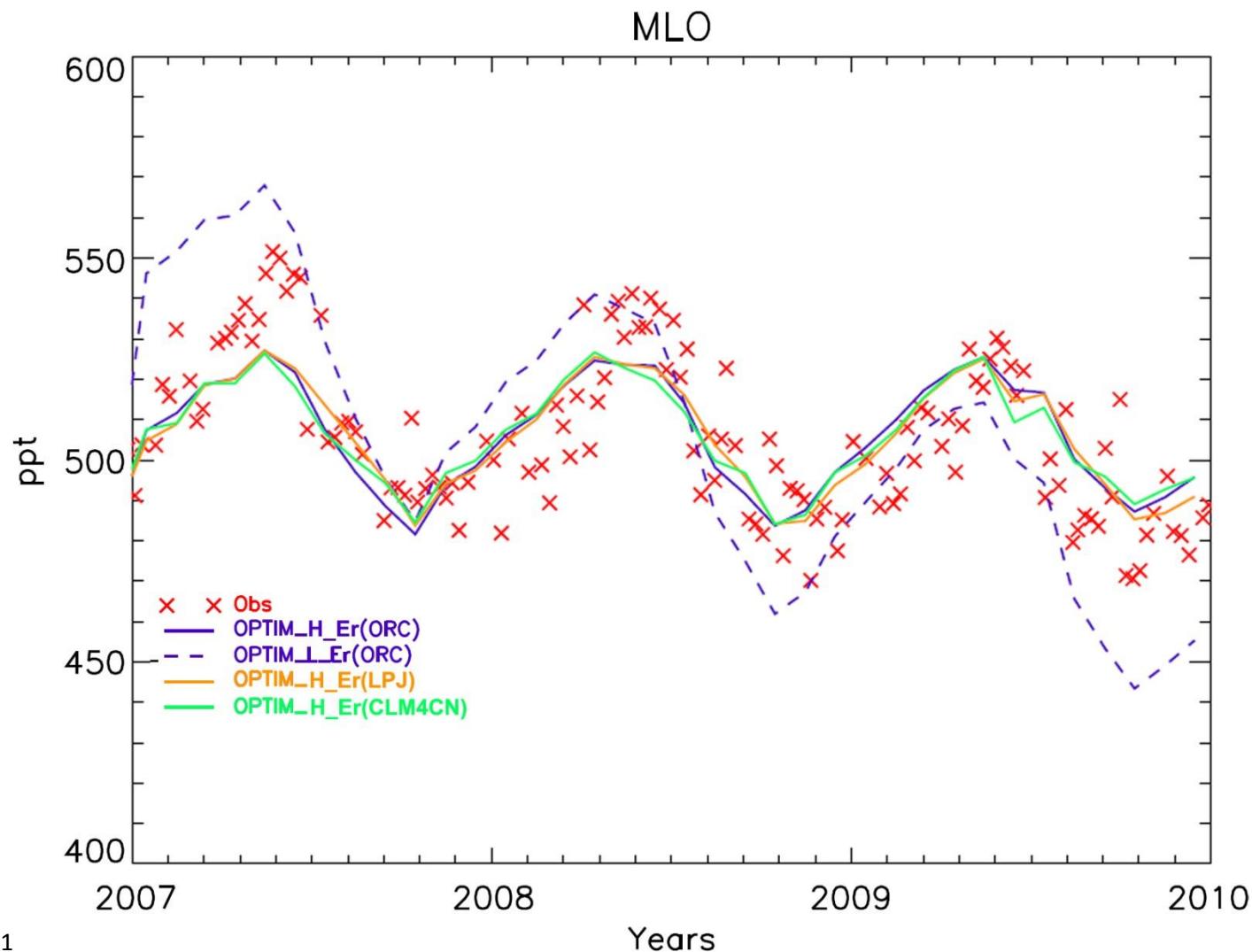
11

12

13

14

Figure 8: Annual variations of OCS monthly mean mixing ratios (in ppt), optimized and monitored at Mauna Loa. Simulations obtained with the LMDz model using the "OPTIM_H-Er" setup (Table 1) applied to ORC, NCAR-CLM4 and LPJ models. Observations (red crosses) are from NOAA-ESRL global monitoring network (Montzka et al., 2007). A sensitivity test was carried out using ORC and the "OPTIM_L-Er" setup (dashed blue line).
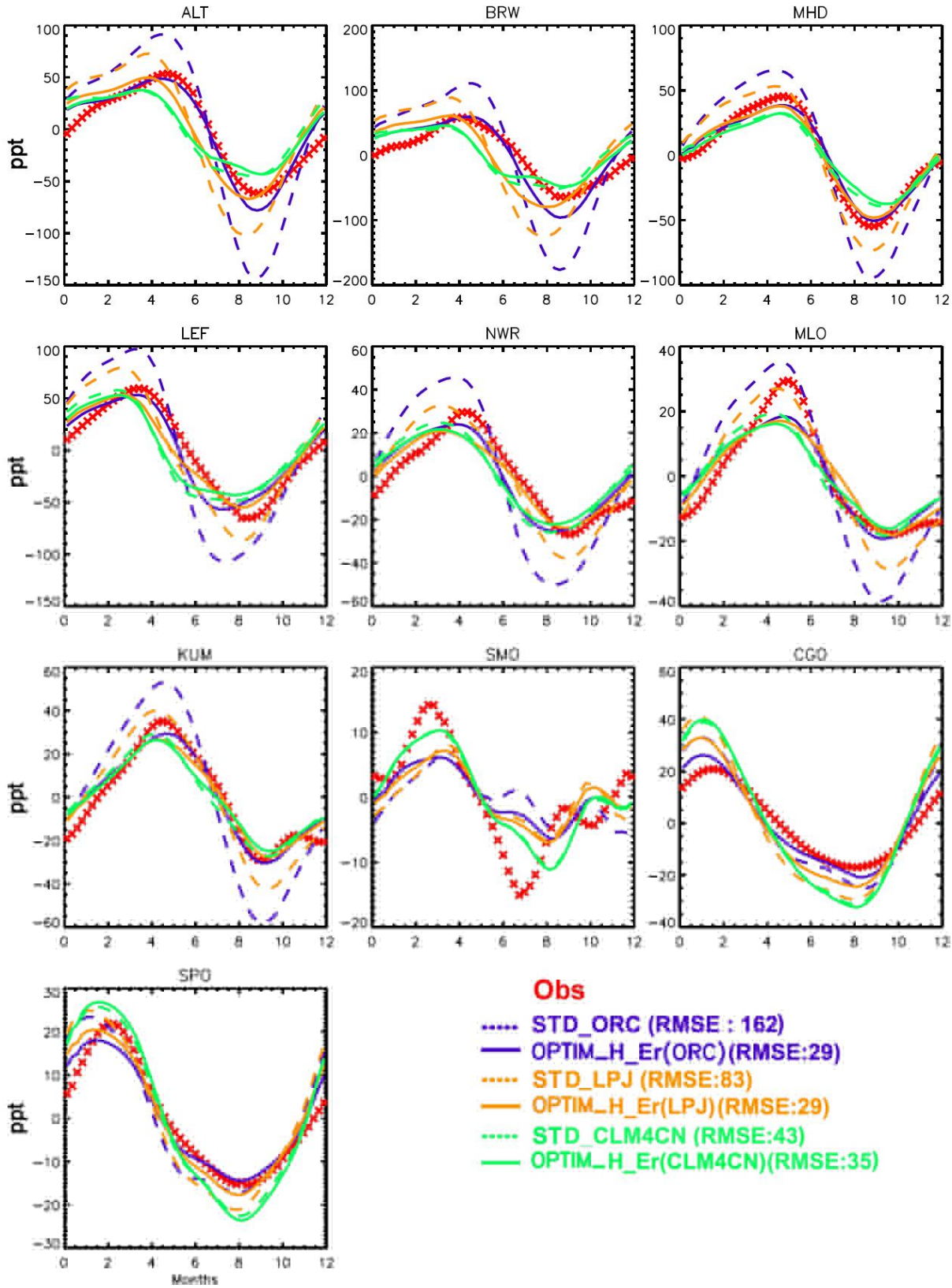
Figure 9: Smoothed seasonal cycles of OCS monthly mean mixing ratios, simulated at 10 stations of the NOAA monitoring network, and obtained after removing the annual trends. Forward simulations with the LMDz model use surface fluxes from the "STD_ORC", "STD_CLM4CN" and "STD_LPJ" setups (dashed lines). The "OPTIM_H-Er" setup (Table 1) was used in the optimizations (solid lines). Observations (red

crosses) are from NOAA-ESRL global monitoring network (Montzka et al., 2007). Global root mean square
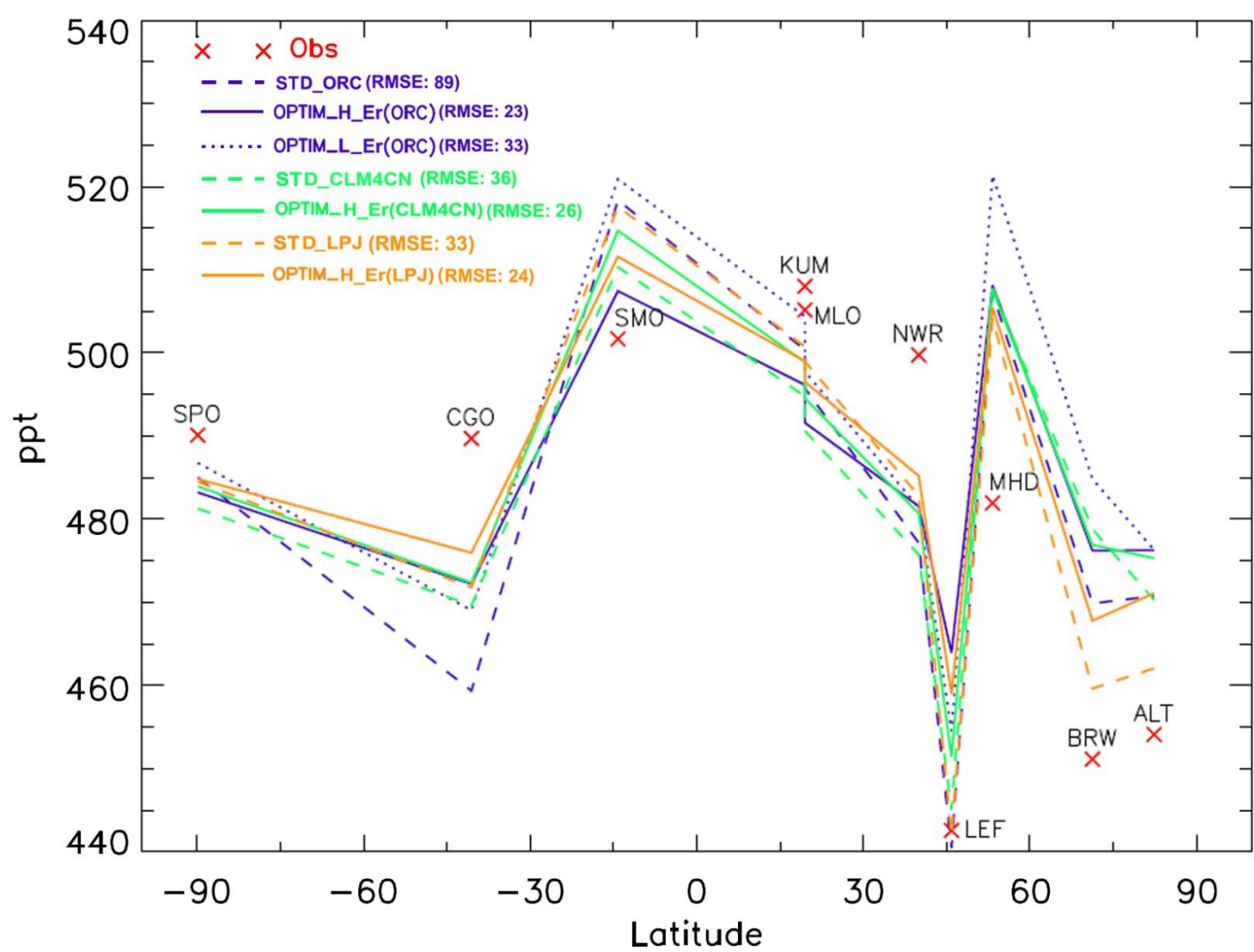
2 errors (MSE) are given in the legend.

4 Figure 10: Differences in OCS annual mean mixing ratios between 10 stations of the NOAA monitoring

5 network, plotted as a function of latitude, for observations (red crosses surmounted by station acronyms)

6 and simulations (no symbol, forward approach (colored dashed lines), inverse approach (colored solid

7 lines)). Forward simulations with the LMDz model use the "STD_ORC", "STD_CLM4CN" and

8 "STD_LPJ" setups (dashed lines). The "OPTIM_H-Er" setup (Table 1) was used in the optimizations (solid

9 lines). A sensitivity test was carried out using ORC and the "OPTIM_L-Er" setup (blue dotted line). Note

10 that the global mean for each simulation ensemble has been set to the global mean of the observations.

11

12

13

14

1

2

3

4

5
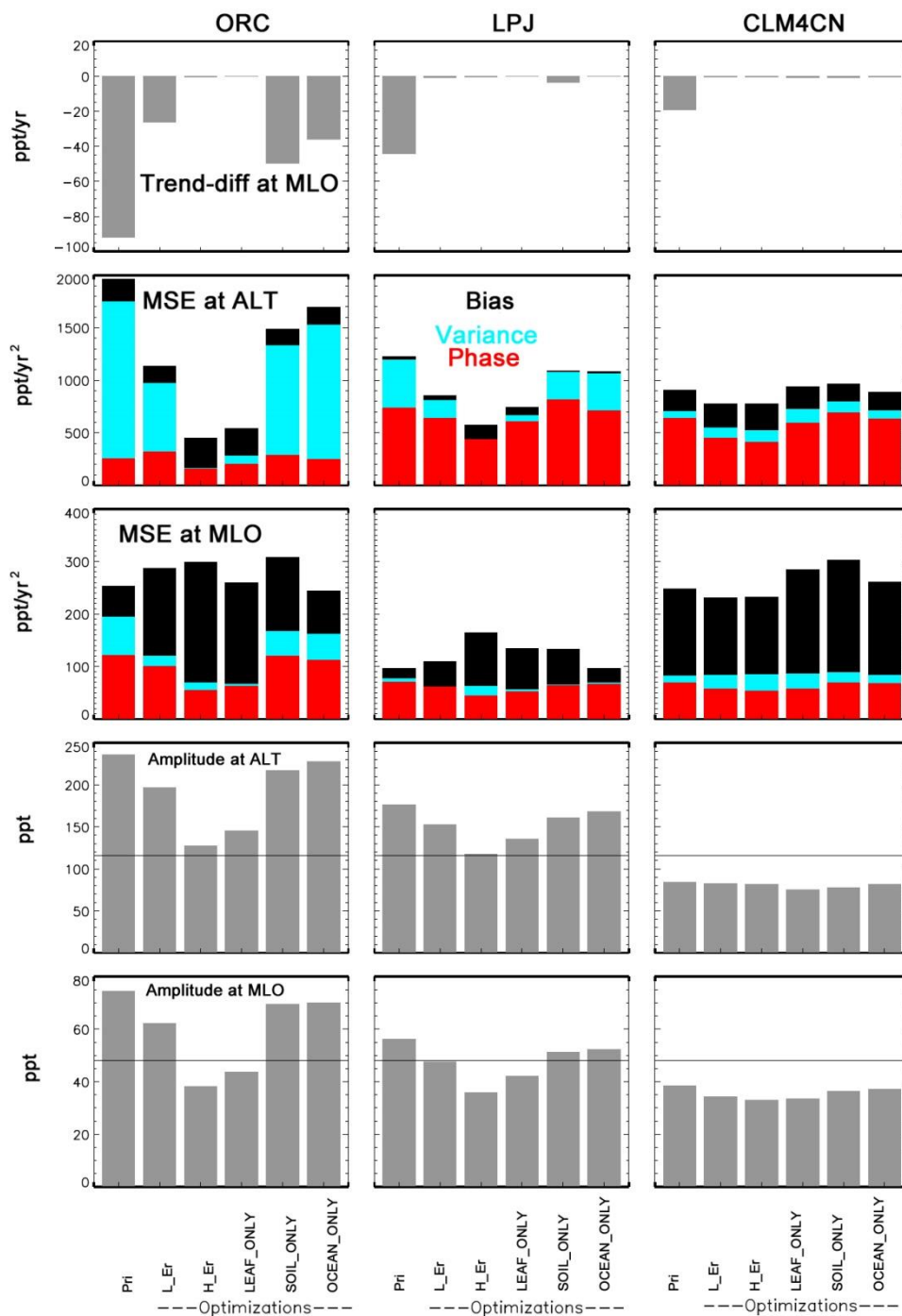
Figure 11: Upper row: differences in annual trends (in ppt yr^{-1}) between simulated monthly mean OCS mixing ratios and measurements, at Mauna Loa. Second and third rows: analysis of smoothed seasonal cycles in simulations and observations (at Alert and Mauna Loa, respectively), and calculation of the mean square error (MSE, in ppt^2) decomposed into three components (bias, phase and variance, as described by Kobayashi and Salam (2000). Fourth

1 and fifth rows: specific analysis of the amplitude of simulated smoothed seasonal cycles, at Alert and Mauna Loa

2 respectively. The horizontal solid line represents the observed value. The bar plots compare the forward approach

3 ("Pri" using the "STD_ORC", "STD_LPJ" or "STD_CLM4CN" setups) to the optimization runs (using the

4 "OPTIM_H_Er", "OPTIM_L_Er", "OPTIM_Leaf_ONLY", "OPTIM_Soil_ONLY" and "OPTIM_Ocean_ONLY"

5 setups (Table 1)).
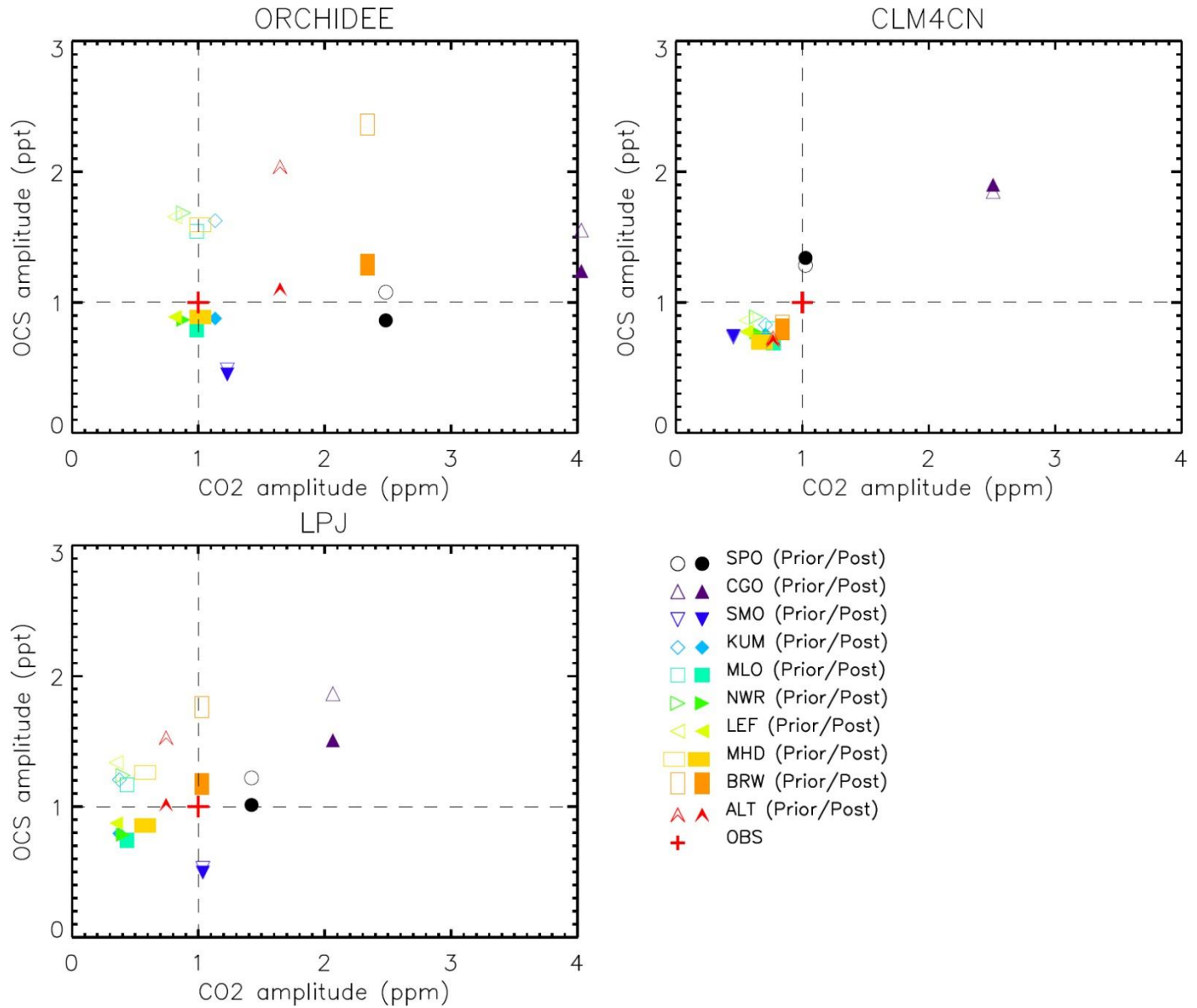
Figure 12: Scatter plots of normalized amplitudes of smoothed seasonal cycles of OCS versus those of CO_2, before (open symbols) and after optimization (filled symbols) of OCS fluxes at 10 stations of the NOAA monitoring network, obtained from the "STD_ORC", "STD_CLM4CN" and "STD_LPJ" setups for the forward simulations and the "OPTIM_H-Er" setup for the optimizations, over the period 2006-2010. Since the amplitude of the seasonal cycle in the observations at each site is used to normalize that of the simulations, the normalized amplitude of observations is 1 (red cross). Hence, a linear translation along the Y-axis towards $Y = 1$ characterizes the optimization process.

1

2

3

4

5

6 **APPENDIX**

7 **A.1 Oceanic emissions of OCS**

8 *Direct emissions:*

9 The main production pathway of OCS is photochemical, hence light dependent and favored by UV-absorbing
10 chromophoric dissolved organic matter (CDOM). The second pathway, the so-called "dark production", is
11 temperature and organic-matter dependent. The two removal processes are hydrolysis (pH-dependent) and ventilation
12 (dependent on temperature and wind speed). In the standard run defined by Launois et al. (2014), the direct emissions
13 of OCS were equal to 813 Gg S yr^{-1}, with 45% of emissions coming from the tropical ocean, but other scenarios (with
14 different sets of parameters) yielded marine fluxes in the range 573 – 1763 Gg S yr^{-1}. To represent the high levels of
15 uncertainty on the marine OCS emissions, an allowed range of variation of 70-150% of the standard run was used in
16 the optimization runs (Table 2).

17 *Indirect emissions:*

18 As suggested by Barnes et al. (1994), OCS accounts for 0.7% of the oxidation products of DMS. Since DMS exhibits
19 a short residence time (Koch et al., 1999; Chin et al., 2000; Kloster et al., 2006), here we assumed that 0.7% of the
20 marine emissions of DMS were instantaneously converted into OCS. For that, we used a new version of the prognostic
21 module developed by Belviso et al. (2012) to compute seawater DMS concentrations and DMS air-sea fluxes. This
22 module, embedded within NEMO-PISCES as that of OCS, improves the representation of DMS dynamics in
23 subtropical waters (Masotti et al., in press)

24 CS_2 emissions from oceans were not computed with NEMO-PISCES but taken from Kettle et al. (2002). We here
25 assumed that 87% of the marine emissions of CS_2 were instantaneously converted into OCS annually (Barnes et al.,
26 1994).

27

28 **A.2 Leaf uptake of OCS**

29 Atmospheric OCS follows the same path as CO_2 to enter the leaves through stomata. However, since OCS is relatively
30 heavier and larger than CO_2, it diffuses less rapidly within the leaf (Berry et al., 2013, and references therein). As
31 proven by laboratory and field studies, the leaf relative uptake of OCS compared to CO_2 (LRU) is species-specific and

highly variable, especially for C4 plants (maize, millet, …) for which the first product in carbon fixation during photosynthesis is realized on a 4-carbon molecule) (Sandoval-Soto et al., 2005; Seibt et al., 2010). Nevertheless, major efforts have been made to estimate the relative deposition rates of OCS and CO_2 (Sandoval-Soto et al., 2005 and 2012; Campbell et al., 2008; Seibt et al., 2010; Stimler et al., 2010).

Here, we used the results of the study from Seibt et al. (2010) who estimated a global average value for k_{LRU} of 2.8 (±10%). This estimate is, however, in the upper range of several estimates, since Sandoval-Soto et al. (2005), Stimler et al. (2012) and Berkelhammer et al. (2013) measured values between 1.45 and 3.03 (±20 to 30%) for different species. In the Seibt et al. (2010) study, estimated LRUs for the different biomes were in the range 1.55 (xerophytic woods and scrub) to 3.96 (cool/cold deciduous forests).

A map combining Köppen-Geiger climate zones with phenology-type from satellite land-cover data provided by the MODIS instrument was used to determine the major plant functional type for each region (Poulter et al., 2011, Kottek et al., 2006). Each species was assigned to a Plant Functional Type (PFT) on the previously described map and then assigned the corresponding k_{LRU} relative uptake value from Seibt et al. (2010). The resulting global mask of k_{LRU} was then used to scale the GPP from the three DGVMs to obtain three different global seasonal OCS uptake fluxes by plants.

A.3 OCS uptake by oxic soils

The approach relies on atmospheric observations that suggest that OCS uptake by oxic soils is proportional to H_2 uptake by these soils. H_2 uptake by soils, which represents about 80% of its total atmospheric loss, is believed to be driven by high H_2-affinity *streptomyces* bacteria (Constant et al., 2010). OCS-degrading activity in heterotrophic soil-bacteria was associated with isolates belonging to the genera *Mycobacterium* (Kato et al., 2008). *Streptomyces and Mycobacterium* are two important genera of the *Actinobacteria* taxon. Recent studies in genetics and cell biology of *Streptomyces* and *Mycobacterium* have revealed striking similarities in the developmental and morphological hallmarks of their life cycles (Scherr and Nguyen, 2009). Moreover, optimal conditions for OCS (Van Diest and Kesselmeier, 2008) and H_2 soil uptake (Smith-Downey et al., 2006), are rather similar: they both exhibit a broad temperature optimum between 20 and 30°C (for most soil types) and soil uptake is optimal for low soil moisture (15-25% of saturation levels). Strong similarities between nighttime deposition velocities of OCS and H_2, in terms of annual mean and ranges of variation, were also inferred from semi-continuous atmospheric observations in a semi-urban site located 20 km SW of Paris, France. When plotted against H_2 data, the OCS deposition velocities were roughly distributed around the 1:1 line (Belviso et al., 2013), but this relationship should perhaps not be applied at the global scale since the deposition velocities recorded in this semi-urban system were in the lower range of deposition velocities recorded by others. However, the airborne measurements carried out by H. Chen above the United States provide support for the existence of such a relationship at the continental scale (H. Chen pers. com.), but the slope of the relationship was only about 0.5. Overall, we choose the value of 0.75 for our standard simulations.

soil uptake of H_2: v_{H2} parameter in equation 3

Two different approaches for estimating v_{H2} are used here. The first one is that from Morfopoulos et al. (2012) who implemented a hydrogen uptake module in the LPJ-WHyME model, including a description of atmospheric H_2 diffusion through soil (Fick's first law) and of the biological processes of uptake which are limited by soil temperature and soil water content. The second approach is that from Bousquet et al. (2011) where an atmospheric inversion model of global and regional fluxes is used, based on a global network of flask observations of H_2 concentration.

A.4 OCS emissions by anoxic soils

OCS emissions by anoxic soils are largely based on the recent inventory by Whelan et al. (2013). Anoxic soil types were mapped accordingly to the representation used in the work by Wania et al. (2010) to represent seasonal methane emissions, as simulated using the LPJ-WHy-ME model. This way, anoxic soils activity were located via methane emissions and translated into hot spots of OCS emissions from anoxic soils, with similar temporal and spatial patterns. Each anoxic soil grid cell was associated the mean value for the anoxic soil OCS emission found in Whelan et al. (2013). However, because of the large uncertainties associated with the OCS flux inventories (see Fig. 3 in Whelan et al. (2013), "soil only" case), we finally assigned zero emission of OCS to rice paddies and 25 pmol m^{-2} s^{-1} to peatlands. Also note that unfortunately, salt marshes, which are strong emission sites of OCS (Whelan et al., 2013), are not taken into account in the LPJ-WHy-ME model.

A.5 DGVMs used and the TRENDY experiment

We used the GPP simulated by three different models (ORCHIDEE, LPJ, CLM4CN) for a specific inter-comparison exercise, TRENDY, in order to derive the leaf uptake of OCS. We use monthly mean outputs from a so-called "S2" simulations, which indicates that the DGVMs were run with the same meteorological forcings (CRU-NCEP dataset, see sitch et al. 2014) and changes in the atmospheric CO_2 concentration, following the 20th century increases. Note that LPJ and ORCHIDEE models were provided originally at 0.5° x 0.5° spatial resolution and CLM4CN at 1.875° x 2.5° spatial resolution. For our study we aggregated the fluxes at the transport model resolution (3.7° x 2.5° spatial resolution).

The DGVM runs have been executed with a constant land use mask and disturbance turned off, which is supposed to represent the impact of climate and CO_2 only on the system. The GPP and Net Ecosystem Exchange (NEE) monthly outputs from these TRENDY simulations have been taken for the 2000-2009 period. In the present paper, we focus on the phase and amplitude of the GPP seasonal cycle from each model. Note that we have used the NEE from each model to compute also the atmospheric CO_2 concentrations at the same stations than for OCS. .

A.6 Optimization: Set up and details about the cost function

Optimization set up:

The optimization relies on the use of the LMDz transport model that relates the surface fluxes to be optimized to the observed atmospheric concentrations. We used pre-calculated transport fields as in Peylin et al. 2005, where the outputs from the LMDz transport model were only saved on a monthly time-step. For each monthly mean observation, we selected the closest monthly mean simulated concentration to compare with. The optimized fluxes correspond to all sources and sinks of Table 2, to which the scaling coefficients are applied for each corresponding flux component.

For each parameter (scaling coefficient of a flux), we assigned a possible range of variation as well as a prior error (1-sigma standard deviation). In the standard configuration, prior parameter values equal to 1.00 and their prior uncertainty was set to 0.3 while the range of variation was set to ±50%, except for the direct oceanic emissions which has a range of variation from -30% to +50% and an error kept to 30%, and the OCS emitted through biomass burning and anthropogenic activities which have a range of variation of ±10% and an error of 10%.

These relatively large errors, combined with the range of variations defined for each flux component (section 2.2), account for current uncertainties on the OCS processes that control the different sources and sinks. We also performed sensitivity tests for the optimization (see Table 3), using a limited 10% error and restricted ranges of variation for all scaling factors (±10%), referred as the Low-Error optimization scenario ("OPTIM_L-Er"). This theoretical test would assume that our OCS flux models (leaf and soil uptake, ocean release, etc.) are accurate which would in turn reveal the potential biases in the simulated atmospheric OCS levels (phase, amplitude, trend) due to other drivers of the OCS signal, such as GPP fluxes and transport model errors. The main objective is indeed to reveal any remaining biases (after the optimization), which could suggest corrections to the GPP fluxes, underlying the OCS leaf uptake model.

The different observations are assigned different weights in the optimization algorithm, represented as observation monthly errors. The choice of this so-called "observation error" is however difficult. It should gather the measurement error as well as the model error including the flux model error, the transport model error and the representation error (scale mismatch between the observed concentration at a given location and the model concentration at coarse scale. Usually the measurement error is relatively small compared to the modeling error. A proper assessment of model error could be done with the use of different models with different parameterizations. However, for transport modeling studies this is usually not feasible and simpler approaches are used. As a first approximation, we used the RMSE of the prior model-observation concentration differences at each station. We choose this simple approach and further averaged the RMSE by latitudinal bands to avoid the complexity of longitudinal differences in model skills. In this case, high-latitude stations such as ALT were displaying large prior MSE (nearly 2000 ppt² year^{-1}, see Fig. 11)) and were therefore assigned with a large observation error in the inversion. Note finally that we took slightly larger errors to account for the fact that the "observation error matrix" in the inversion is assumed diagonal and thus neglect all error correlations. However, we have done several sensitivity tests and in particular with equal observation errors between stations (set to 18ppt), which did not lead to significantly different messages. Overall, the observation errors are set to a high value in Northern Hemisphere stations (26 ppt), while stations from tropical regions are assigned 20 ppt error and extra-tropical stations from the Southern Hemisphere are assigned 13 ppt error (these regions being mostly influenced by oceanic fluxes).

Cost function:

The first term of $J(x)$ represents the weighted data-model squared deviations, i.e. the misfit between the simulated outputs and the corresponding observational data. The second term represents the mismatch between optimized and prior values, weighted by the prior uncertainties on parameters. The **R** matrix correspond to the observation error described above. Correlations in **R** are too difficult to assess and therefore neglected. Uncertainties on the a priori flux scalar values (**B** matrix) are set to large values (see below) which minimizes the influence of this term in the cost function. Moreover, error correlations between a priori parameter values were also neglected.

Given that we optimize scalars of the OCS surface fluxes and that the OCS destruction by OH in the atmosphere is fixed (i.e., prescribed and independent of the atmospheric OCS concentrations), the optimization problem is linear (i.e., the atmospheric concentrations linearly depend on the surface fluxes and their scaling factors). **M(x)** is thus equal to **M.x**, with **M** now representing the pre-calculated model concentration sensitivities to surface fluxes. With this assumption, the minimum of the cost function can be obtained directly with a matrix formulation of the inverse problem (see for instance Tarantola, 1987).

Note that in order to account for bounds on each flux parameter (to limit the optimal value in the prescribed range of variation), we iterated the scheme seven times. At each of the iterations, the optimized value for each parameter may be outside its range of variation. In this case, we fixed the parameter value (flux scalar) to its boundary and re-optimized excluding the parameter from the optimization. We then repeated the process until all parameters were fixed or within their range of variations. Note finally that assuming Gaussian errors allows to estimate the posterior error covariance matrix on the parameter from a matrix formulation (see Tarantola, 1987) and thus to compute error correlations..

A.7 Simulated surface fluxes: regional and seasonal details of the obtained emissions and uptakes

Direct oceanic emissions:

Photoproduction and hydrolysis are the main drivers of the mid and high latitude flux seasonality of both hemispheres: oceans take up OCS from the atmosphere in winter (Fig. 1, top), whereas summer fluxes are largely positive, between 3 and 10 pmol m^2 s^{-1}.

The tropical regions (30°S-30°N) represent 45% of the yearly global OCS emissions and stay rather constant throughout the year (6 to 8 pmol m^2 s^{-1}). There, the major controlling factors are light and sea-surface temperature (SST) through SST-mediated dark production of OCS (Launois et al., 2014). Note the presence of an OCS emission "hot spot" off the coast of Somalia in July (up to 25 pmol m² s^{-1}), a feature linked to intense upwelling simulated by the NEMO-PISCES model on which our marine emission maps rely.

Indirect oceanic emissions

Global maps of OCS emissions from DMS atmospheric oxidation for the months of January and July are provided in the supplementary material (Fig. A1). Most of the OCS indirect emissions occur at high latitudes in the Southern Hemisphere, regions where the amplitude of the seasonal cycle is also the most important, with seasonal emissions varying between 4 and 7 Gg S per month (Fig. A1).

1   The OCS emissions based on the CS_2 fluxes are mostly emitted in tropical regions, based on the CS2 flux maps by

2   Kettle et al. (2002). These fluxes present a larger seasonal amplitude in the extra-tropical regions than in the tropics.

Oxic soil uptake of OCS

4   The sensitivity of monthly soil OCS uptake rates to the different parametrizations (H_2 uptake and the ratio of OCS to

5   H_2 deposition velocity) is evaluated in Fig. A2, at the global scale and by large bands of latitude. The largest total

6   uptake of OCS by oxic soils is obtained using the "TEST_SOIL_MORF_1:1" scenario (700 Gg S yr^{-1}, with a ratio of

7   OCS to H_2 deposition velocity of unity. The smallest total uptake of OCS by oxic soils is obtained using the

8   "TEST_SOIL_BOUSQ_0.5:1" scenario (330 Gg S yr^{-1}).

9   Whatever the magnitude of the ratio between deposition velocities, the seasonal variations are more important in the

10   extra-tropical areas of the Northern Hemisphere than elsewhere, and they differ between models of H_2 deposition rates

11   ("TEST_SOIL_BOUSQ" versus "TEST_SOIL_MORF"). Indeed, in "TEST_SOIL_BOUSQ" the OCS sink reaches a

12   peak in spring whereas maximum uptake rates are seen in summer in "TEST_SOIL_MORF". Using the

13   "TEST_SOIL_MORF_1:1" scenario, the extra-tropical areas of the Northern and Southern Hemispheres each account

14   for 30% of total uptake, and the remaining is taken up by tropical regions. Using the "TEST_SOIL_BOUSQ_0.5:1"

15   scenario, the extra-tropical areas of the Northern and Southern Hemispheres, and the tropical regions account for 53%,

16   29% and 18% of the total uptake, respectively.

Soils net fluxes of OCS

18   At the global scale, the monthly fluxes of OCS vary between 0 and -28 Gg S per month (using Bousquet et al., 2011

19   for H_2 flux) and between -15 and -28 Gg S per month (using Morfopoulos et al., 2012 for H_2 flux). These large soil

20   flux seasonal variations will impact the simulated OCS atmospheric seasonal variations. We also notice that for all

21   configurations, the largest amplitude of the OCS flux variations are found in the Northern Hemisphere.

22   Using the "TEST_SOIL_BOUSQ_1:1" configuration, the simulated fluxes vary between +1 and -15 Gg S per month

23   in the Northern Hemisphere (Fig. A2), while they range between +3 and -8 Gg S per month using

24   "TEST_SOIL_MORF_1:1". In the tropics, the simulated fluxes also display large variations (between -2 and -8 Gg S

25   with "TEST_SOIL_MORF_1:1", between -11 and -14 Gg S per month with "TEST_SOIL_BOUSQ_1:1"). The same

26   configurations lead to variations respectively between -3 and -12 Gg S per month and between -7 and -11 Gg S per

27   month in the Southern Hemisphere.

Plant uptake of OCS

29   Because OCS uptake by plants is represented in our models as a linear function of GPP (Eq. 2), the phase and

30   amplitude of the seasonal variations in OCS plant uptake and GPP have the same patterns.

31   The ORC model displays stronger OCS uptake than the other models, throughout the year and especially during the

32   summer months (Fig. A3) due to its larger GPP. In ORC, the extra-tropical regions of the Northern Hemisphere are

33   responsible for this summer uptake and account for about a third of the total plant uptake. The uptake of OCS in

34   tropical regions is roughly constant and accounts for 45% of the total uptake. The remaining 20% is contributed by the

extra-tropical regions of the Southern Hemisphere where the intensity of the summer maximum (about 35 Gg S month^{-1}) is roughly a quarter of that occurring in the Northern Hemisphere. Fig. A3 reveals large differences in the amplitude of seasonal variations depending on which biospheric model is used to model the leaf uptake (the respective seasonal amplitudes are between 50 and 95 Gg S per month for ORC and CLM4CN). Large differences in the modeled OCS level seasonal phase can also be seen. Indeed, plant uptake reaches a peak in late spring in CLM4CN while maximum uptake occurs later in the year in the other models (the time lag is about two months).